KERNFORSCHUNGSANLAGE JÜLICH
GESELLSCHAFT MIT BESCHRÄNKTER HAFTUNG

Surface Phenomena of Thermionic Emitters

„Round Table Conference"
held on June 10, 1969 in the
„Institut für Technische Physik
der Kernforschungsanlage Jülich GmbH"

Jül - Conf - 3
November 1969

Als Manuskript gedruckt

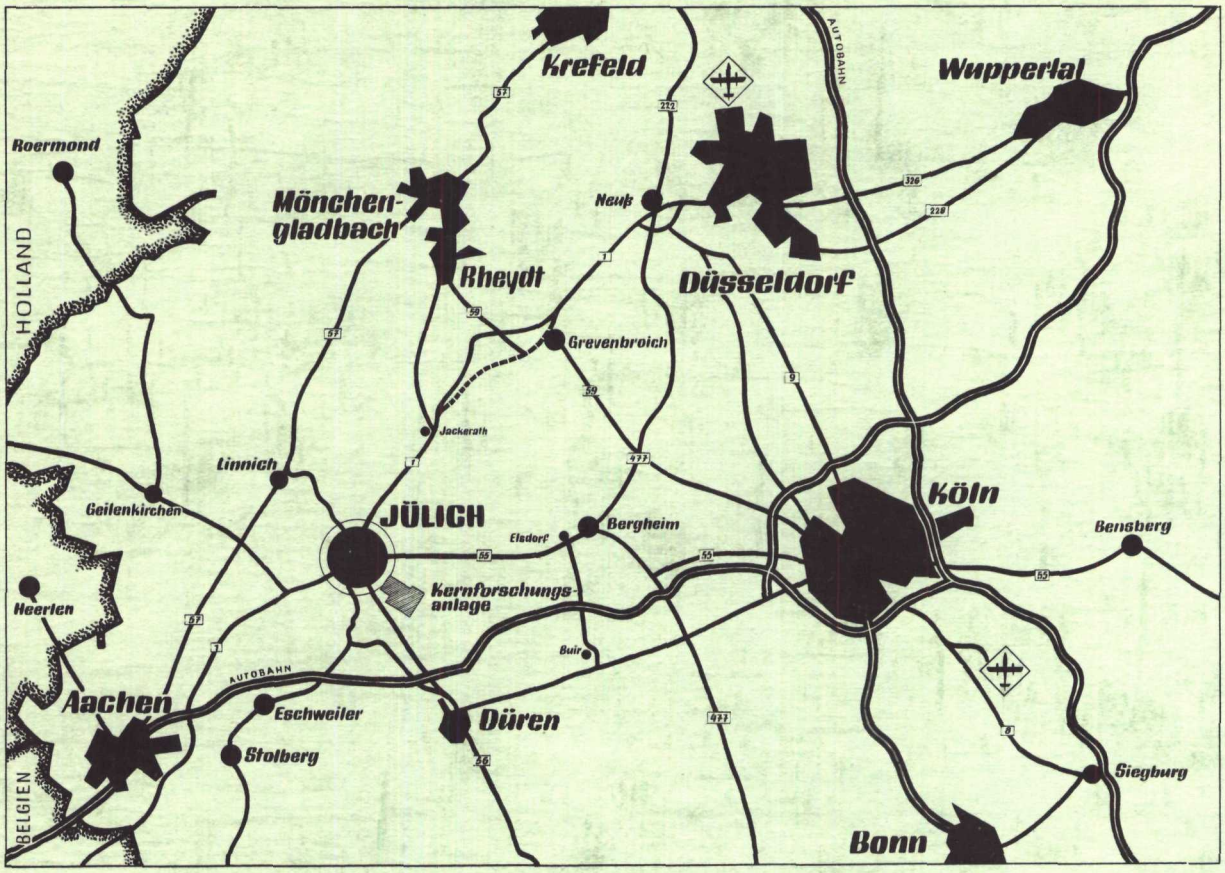

Berichte der Kernforschungsanlage Jülich – Jül – Conf - 3

Dok.: Thermionic Emitters - Conferences
Conferences - Federal Republic of Germany
Thermionic Emitters - Surface Phenomena
Thermionic Emitters - Materials

DK: 537.58 : 061.3
65.012.63 (430.2)
537.58 : 532.6
537.58.002

Zu beziehen durch: ZENTRALBIBLIOTHEK der Kernforschungsanlage Jülich GmbH,
Jülich, Bundesrepublik Deutschland

Conf-690637--

Surface Phenomena of Thermionic Emitters

„Round Table Conference"
held on June 10, 1969 in the
„Institut für Technische Physik
der Kernforschungsanlage Jülich GmbH"

Foreword

A "Round-Table Conference" on surface phenomena of thermionic emitters was held on June 10, 1969 in the "Institut für Technische Physik" of the Kernforschungsanlage Jülich GmbH. This meeting was a sequel to a similar one organized on July 7, 1967 by Dr. Devin in Saclay (C.E.A.). This conference gave emphasis to the great importance which in our opinion must be given to the surface properties of thermionic emitters in order to yield high efficiency and long lifetime converters. The international interest in this conference as well as the general result of the presentations and the vital discussions which followed, have supported this opinion in every respect.

This volume contains those papers for which written presentations were submitted by the authors.

I would like to thank Dr. H. Wagner for carrying out the editorial work associated with assembling this report and also Miss J. Gollnick for typing the manuscripts.

Prof. Dr. Ernst A. Niekisch

List of Participants

Dr. T. Alleau	Centre d'Etudes Nucléaires de Saclay
DP. Batzies	Brown, Boveri & Cie., AG Heidelberg
Dr. J. Bohdansky	Euratom Ispra/Italy
Dr. M. von Bradke	Deutsche Versuchsanstalt für Luft- und Raumfahrt e.V.
Dr. Devin	Centre d'Etudes Nucléaires de Saclay
Dr. F. Forstmann	University of Cambridge
DP. Gregorius	Siemens AG, Erlangen
DP. G. Haufler	Institut für Kernenergetik der Universität Stuttgart
Prof. Heiland	II. Physikalisches Institut der Technischen Hochschule Aachen
Dr. B.J. Hopkins	University of Southampton
DI. A. Koeppe	Institut für Kernenergetik der Universität Stuttgart
Dr. K. Müller	Institut für Angewandte Physik der Universität Karlsruhe
Dr. Mönch	II. Physikalisches Institut der Technische Hochschule Aachen
Dr. Peehs	Siemens AG, Erlangen
Dr. Pruschek	Institut für Kernenergetik der Universität Stuttgart
Dr. D. Schmidt	Deutsche Versuchsanstalt für Luft- und Raumfahrt e.V.

Dr. Schretzmann	Institut für Neutronenphysik und Reaktortechnik des Kernforschungszentrums Karlsruhe
Dr. A.M. Shroff	Thomson-CSF, Etablissement de Corbeville
Dr. Venker	Brown, Boveri & Cie., AG Heidelberg
Prof. E.A. Niekisch Dr. H. Wagner Dr. E. Preuß DP. R. Butz DP. H.A. Claassen DP. W. Erley DP. B. Krahl-Urban DP. S. Lehwald DP. K.G. Tschersich	Institut für Technische Physik der Kernforschungsanlage Jülich GmbH

Contents

W

Cesium Adsorption on Tungsten Studied by Low Energy Electron Diffraction (LEED) and Secondary Electron Spectroscopy

Klaus Müller

Institut für Angewandte Physik, Universität Karlsruhe, Germany

This contribution is based on papers by A.U. Mac Rae, K. Müller, J.J. Lander, J. Morrison, and C.J. Phillips[1]-[4].

Surface structures, work function changes, Auger electron emission and surface plasma losses have been studied in a LEED apparatus for the adsorption of cesium on clean (110) and (100) single crystal planes of tungsten. In such an experiment a well defined beam of slow electrons (less than 100 eV) with a penetration of a few atom layers impinges on the surface of the sample. Emitted secondary electrons have an energy distribution containing all energies between zero and the primary energy. In case of a well ordered surface the elastic part of backscattered electrons appears in discrete diffracted beams which are detected on a fluorescent screen, fig. 1.

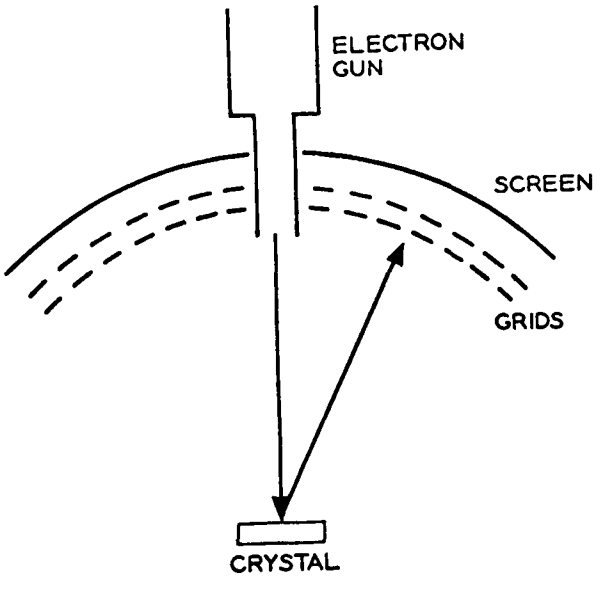

Fig. 1 Schematic of Low Energy Electron Diffraction

In front of the screen there is a set of fine mesh grids which acts as a retarding field energy filter to reject inelastically scattered electrons. The position of diffraction spots on the screen determines the diffraction angle as well as the symmetry and hence determines the unit mesh of the crystal surface. For more detail see the LEED review article by J.J. Lander[5].

The whole unit is mounted in an ultra-high vacuum system and the sample must be cleaned in situ in order to attain a surface free of contamination. The main results of a (100) tungsten surface covered with Cs are given in this report:
The clean tungsten surface held at room temperature in ultra-high vacuum was exposed to a beam of Cs atoms while the surface structure was continuously monitored with LEED. A series of structures was observed as a function of Cs coverage: As a first step low density arrangements of closest approach' develop with increasing Cs coverage into an ionic layer of well defined c(2x2) structure, fig. 2.

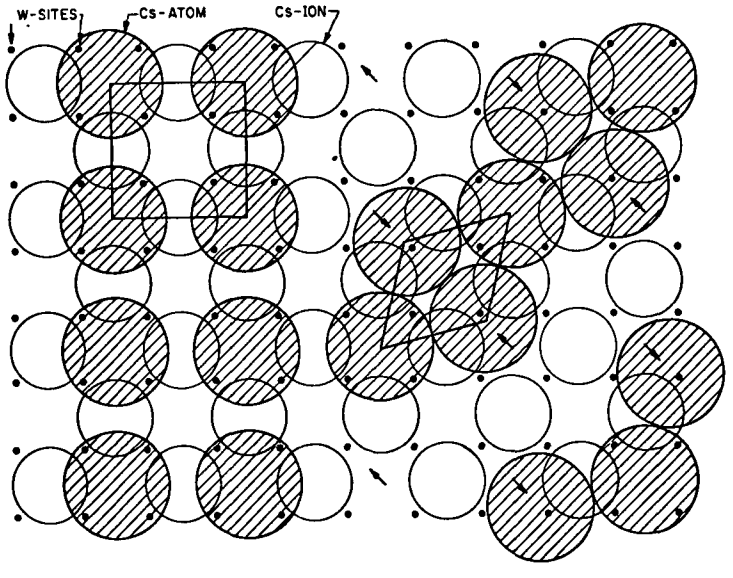

Fig. 2 Various stages for the built up Cs layer on tungsten(100)

This completes a first layer on top of which a second layer develops with two consecutive structures: An intermediate p(2x2) arrangement with adsorption sites assumed to be over

'holes' in the underlying c(2x2) layer which rearranges into a hexagonal close-packed (c.p.) structure as the coverage increases. In the process of rearrangement 1/3 of the atoms remain centered over 'holes' in the first layer while 2/3 are finally centered approximately above points of contact of Cs ions in the first layer. The density of this hexagonal c.p. layer is close to that of bulk Cs. But no third layer is formed at room temperature even with prolonged Cs exposure.

The intermediate 2. layer with p(2x2) structure is, because of its low density, assumed to be in an insulating state with one de-localized electron per atom. The final hexagonal c.p. arrangement, however, is metallic. This is evidenced by the observation of a cesium plasma peak which appears when the intermediate structure begins to rearrange and increases in intensity as the hexagonal array is formed.

The final diffraction pattern contains spots due to all three periodicities, that of the W surface, the ion layer and the c.p. metallic layer. And moreover it contains spots due to linear combinations of these periodicities which indicates multiple scattering of the primary electrons.

Concurrent with the observation of diffraction patterns the change in work function $\Delta\Phi$ versus Cs coverage was measured. The extrapolated cut-off at the low energy side of the secondary electron energy distribution function shifts as the work function of the specimen changes. If other contact potentials involved can be kept constant this shift is equal to $\Delta\Phi$. It is measured by using the grid system as a retarding field analyser and the screen as the detector. The first layer reduces the work function by 2 eV. The minimum in Φ coincides with the completion of the p(2x2) intermediate 2. layer, fig. 3.

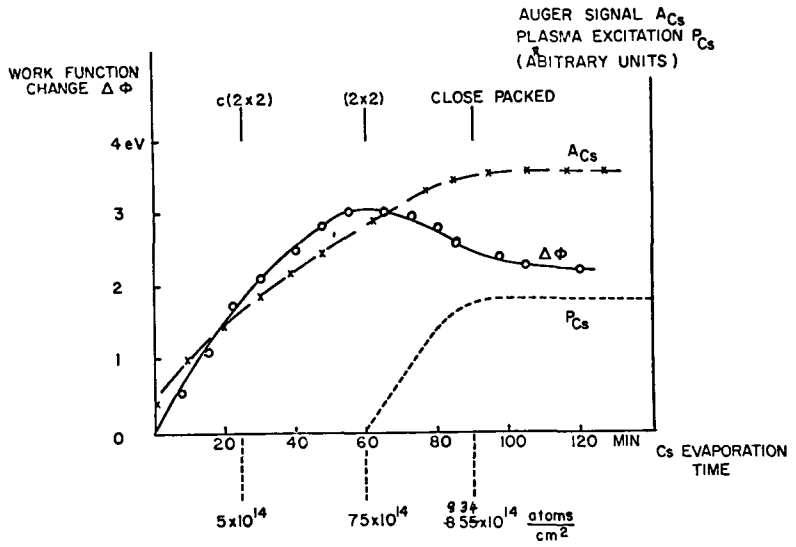

Fig. 3 Work function change, Auger signal and plasma excitation as function of the Cs evaporation time

As the close-packed structure forms the work function increases with its final value 0.3 eV higher than the value found for the minimum. The appearance of a minimum in ϕ is assumed to be a geometrical effect, connected with the intermediate (2x2) layer and its rearrangement into c.p.

The intensity of Auger electrons emitted by cesium was also studied by extracting Auger transitions from the secondary electron distribution function. This again is done using the grids as a retarding field analyser. The Auger signal was found to be increasing as a function of coverage. It levels off to a constant value when the final c.p. stage is reached, thus again indicating that no more Cs is accumulated even with prolonged evaporation. The Auger signal from less than 1/10 of a monolayer could well be detected. Fig. 3 shows the comparison of work function change, Auger emission, plasma excitations and structure data.

(1) A.U. Mac Rae, K. Müller, J.J. Lander, and J. Morrison, to be published in Surface Science

(2) A.U. Mac Rae, K. Müller, J.J. Lander, J. Morrison, and J.C. Phillips, Phys. Rev. Letters 22, 1048 (1969)

(3) J.J. Lander and J. Morrison, Surface Science 14 (1969)

(4) J. Morrison, J.J. Lander, and K. Müller, to be published in J. Vac. Sci. Technology

(5) J.J. Lander in: "Progress in Solid State Chemistry", Vol. II, Editor: H. Reiss, Pergamon 1965

Work Function Measurements of Tungsten Single Crystal Planes with Various Adsorbates

B.J. Hopkins and B.H. Blott

Physics Department, The University of Southampton

Abstract

Kelvin work function measurements have been made during the adsorption of Cs, Ba, U, I_2, Br_2, Cl_2, O_2, H_2, N_2, and H_2O onto (110), (100) and, in some cases, (111) oriented macroscopic tungsten single crystals. Agreement between the Cs results and the predictions of various theoretical models will be mentioned. Over the range Cs to water the atomic adsorption behaviour can be interpreted in terms of very simple ideas based upon electronegativity differences between the three crystal faces and the adsorbed entities. Exceptions to this correlation are H_2 and N_2, where it is thought that penetration into the tungsten lattice may take place with a reversal of surface dipole.

Surface States from Band Structure Calculations

Frank Forstmann

Cavendish Laboratory, Cambridge

Surface states represent electrons bound to the surface. They will determine the electron distribution there and so also the potential near the surface, the dipole layer relevant to work function as well as the interaction with absorbed ions and atoms.

A method for calculating these states in the frame of band structure calculations, that means with a realistic potential, is presented. The electron wavefunction inside the metal is represented as a sum over Bloch waves, which are calculated as in band structure calculations. This wavefunction is then matched to the wavefunction outside. Such a matching is possible only for certain energies, the energies of the surface states. The application to d-band metals is discussed. One can expect surface states in these metals below the Fermi level.

In band structure calculations, one solves the one-electron Schroedinger equation in a periodic potential. The wave vector or crystal momentum of the physical solutions has to be real due to the infinite periodicity. One gets additional solutions by truncating the periodic potential when introducing a crystal surface. The surface states represent electrons bound to the surface with wavefunctions decaying on both sides of it. The electron density in such a state compared to that in a state with real wave vector is N times larger near the surface, where N is the number of layers normal to the surface. So the electron distribution at the surface will be determined by these states.

Surface states have been investigated experimentally on semiconductors for a long time[1] but for metals, only recently in an ion neutralisation experiment on a nickel surface[2] an indication was given that the density of electron states near

the surface could differ appreciably from that of the bulk metal. Such surface states can play a role in field emission, changing the apparent work function. Also adsorbates, gases, ions interacting with the metal surface will mainly see electrons in surface states.

There have been several attempts to calculate surface states. The main conclusions were drawn from one dimensional models[3]+[4]. There was uncertainty about their validity in three dimensions[5]. Most three dimensional models used the tight binding approximation with a certain ambiguity of lots of parameters[6]-[8]. Another method, starting with Bethe[9] and Maue[10] and taken up again by Heine and co-workers[11]-[14] determines the electron states inside the metal by methods of band structure calculations and then tries to match with continuous amplitude and derivative the wavefunction inside to the solutions outside the metal. Such a matching is only possible under certain conditions and for special energy values, the energies of the surface states.

The Schroedinger equation has to be solved in a potential indicated in fig. 1.

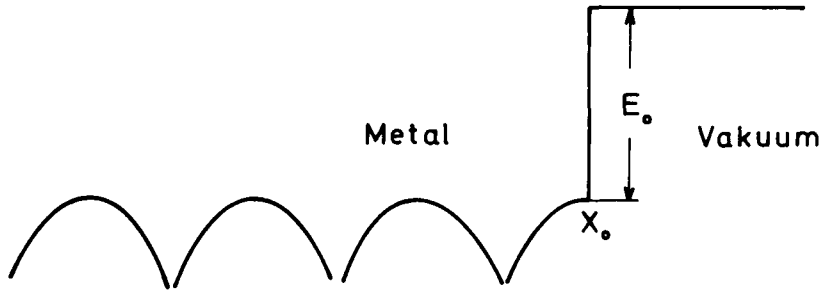

Fig. 1 Potential Model

In y- and z-direction it is infinitely periodic. In principle the wavefunction at a given energy inside the crystal is built up as a sum over an infinite set of Bloch states, outside as a Fourier series. When there are propagating waves inside for this energy, there are just enough coefficients available to effect always a matching at the surface joining a decaying tail outside to all Bloch states. This is not so in a band gap where only the inside decaying solution can be used. There the matching donditions lead to an eigenvalue equation.

The method shall be demonstrated in a simple case. In simple metals the band structure is nearly free electron like (NFE) (fig. 2), that means $E \approx \underset{\sim}{K}^2$ and $\Psi_{\underset{\sim}{K}}(\underset{\sim}{r}) \sim \exp(i\underset{\sim}{K}\underset{\sim}{r})$.

Fig. 2 NFE-Bandstructure

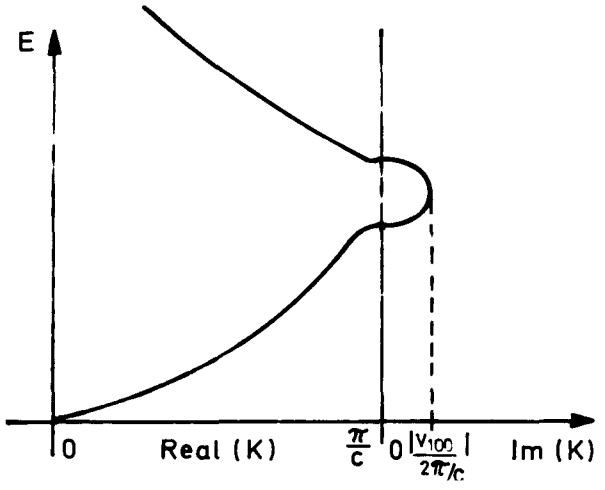

At a band gap, say in the 100 direction of a simple cubic crystal with lattice spacing c, band structure calculations show that a good representation of the wavefunction is given by

$$\Psi_K = \exp(iKx)\left(1 + \frac{|V_{100}|}{(K-\frac{2\pi}{c})^2-E}\exp(-i\frac{2\pi}{c}x)\right)$$

with energy

$$E = \frac{1}{2}\left(K^2 + \left(K-\frac{2\pi}{c}\right)^2\right) \pm \frac{1}{2}\sqrt{\left(K^2-\left(K-\frac{2\pi}{c}\right)^2\right)^2+4V_{100}^2}$$

$V_g = \frac{1}{\Omega}\int \exp(i\underset{\sim}{g}\underset{\sim}{r})\, V(\underset{\sim}{r})d\underset{\sim}{r}$ is the matrix element of the potential, fully determined by comparing the band structure with experiments.

At the band gap $K = \frac{\pi}{c}$, this leads to the following results: If $V_{100} < 0$, the wavefunction is $\cos(\frac{\pi}{c}x)$ at the bottom of the gap and $\sin(\frac{\pi}{c}x)$ at the top. For $V_{100} > 0$ it is vice versa. For the wavefunction in the gap, one is led to the expression:

$$\psi = \exp(Qx)\cos\left(\frac{\pi}{c}x + \delta\right) ,$$

which is a decaying wave between cos and sin. This is a solution of the Schroedinger equation

$$\left(-\frac{\nabla^2}{\nabla} + V(\underset{\sim}{r})\right)\psi = E\psi$$

if

$$Q^2 = \left(E + \frac{\pi^2}{c^2}\right) + \sqrt{4\frac{\pi^2}{c^2}E + V_{100}^2}$$

$$\sin 2\delta = -\frac{\frac{2\pi}{c}Q}{V_{100}}$$

The imaginary part Q of the wave vector is zero at the gap edges and goes through a maximum of $Q_{max} = \frac{V_{100}}{2\pi/c}$. δ varies from 0 to $\pi/2$ for $V_{100} < 0$ and from $-\frac{\pi}{2}$ to 0 for $V_{100} > 0$ for increasing energy throughout the gap.

By knowing the wavefunction inside, one tries to match the wavefunction $\psi = e^{-\sqrt{E_o - E}\,x}$ outside, equating the amplitude and derivative at $x = x_o$, which gives the condition

$$Q - \tan\left(\frac{\pi}{c}x_o + \delta\right) = -\sqrt{E_o - E}$$

where x_o is the midpoint between two atoms and the zero of the coordinates is at an atom centre in order to get the sign of the potential matrix element in accordance with pseudopotential theory. So $x_o = \frac{c}{2}$.

For $V_{100} < 0$, the lefthand side of the equation is always positive throughout the gap showing that no matching of the wavefunctions is possible. For $V_{100} > 0$ the lefthand side covers all negative values and for one special energy, the energy of the surface state, the conditional equation is fulfilled. Thus it results that for $V_{100} > 0$ there is a surface state in the gap, for $V_{100} < 0$ there is none. One can visualize the situation this way:
$V_{100} < 0$ means that the electron lowers its energy when having high density at the atom centres giving the cos-function at the lower band edge. Raising the energy shifts the nodes (fig. 3) to the left, resulting in a derivative which has the opposite sign of that outside, so no matching can occur

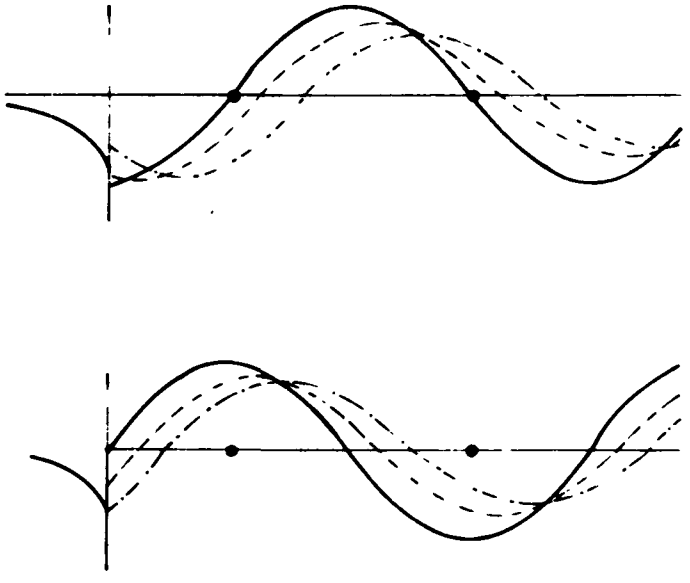

Fig. 3 Wavefunctions in the gap
Upper position $V_{100} < 0$
Lower position $V_{100} > 0$

If $V_{100} > 0$, one starts with sin at the bottom of the gap and by moving the nodes inwards with increasing energy, one finds

now the right slope at the boundary and a continuous amplitude and derivative at a certain energy.

This example was carried through for K normal to the surface. If K varies throughout the two dimensional Brillouin Zone of the surface, one may find a surface state for each direction at varying energy, resulting in a band of surface states. This has been worked out for the 110 face of silicon by Jones[14].

In d-band metals, one has band gaps for certain symmetries inside the energy region, where the d-bands lie. Especially the crossing of the s-band with the d-band of the same symmetry gives such a gap. In copper in the 100 direction it looks like fig. 4.

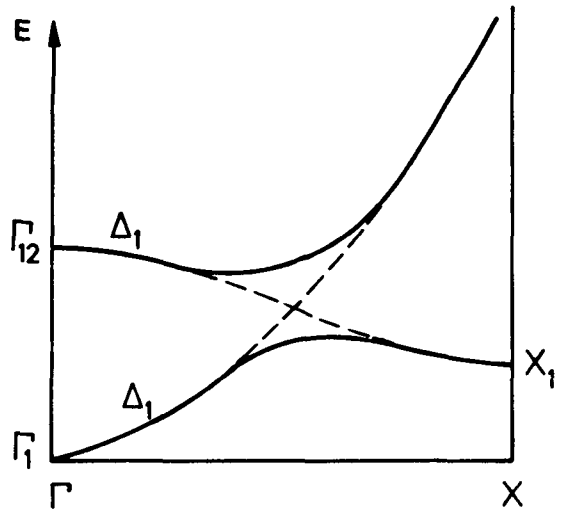

Fig. 4 Bandcrossing in a fcc-d-band metal

In this gap one can look for surface states according to the scheme shown above. One has first to study the complex band structure around the relevant energy[15] and then match the wavefunctions[16].

The calculations show, that there is a surface state in this band gap in copper with an energy close to the lower edge of the gap.

(1) A. Many, Y. Goldstein, and N.B. Grover, Semiconductor Surfaces (North Holland Pub. Co., Amsterdam 1965)

(2) H.D. Hagstrum and G.E. Becker, Phys. Rev. Let. 22, 1054 (1969)

(3) T. Tamm, Phys. Z. Sovjet, 1, 732 (1932)

(4) W. Shockley, Phys. Rev. 56, 317 (1939)

(5) H. Statz, Z. Naturforschung 5a, 534 (1950)

(6) E.T. Goodwin, Proc. Camb. Phil. Soc. 35, 205, 221, 232 (1939)

(7) J. Koutecky, J. Phys. Chem. Solids 14, 233 (1960)

(8) J. Koutecky and M. Tomasek, Surf. Science 3, 333 (1965)

(9) H. Bethe, Ann. Phys. 87, 55 (1928)

(10) A.W. Maue, Z. Phys. 94, 717 (1935)

(11) V. Heine, Proc. Phys. Soc. 81, 300 (1963)

(12) V. Heine, Surf. Science 2, 1 (1964)

(13) R.O. Jones, Proc. Soc. 89, 443 (1966)

(14) R.O. Jones, Phys. Rev. Let. 20, 992 (1968)

(15) J.B. Pendry and F. Forstmann, to be published in J. Phys.

(16) J.B. Pendry and F. Forstmann, to be published in Z. Phys.

The Influence of Interstitially Dissolved Oxygen and Carbon Atoms on the Work Function of Zirconium

Gunther Haufler, Rolf Mayer, and Hans Goretzki

Institut für Kernenergetik der Universität Stuttgart, Max-Planck-Institut für Metallforschung, Institut für Sondermetalle

The solid solutions and compounds of nonmetals (C,N,O) and transition metals of the early groups with half filled d-electron shells are characterized by a close packed arrangement of the atoms. The metalloid atoms occupy the interstitial sites of the metal lattice which usually forms cubic face or body centered and hexagonal structures. Since these materials show metallic properties according to the electrical resistivity and thermal conductivity they can be described by the metallic band model. In relation to their application for thermionic converters it is of particular interest to study the influence of the interstitial atoms on the work function of these materials. These investigations can be easily performed since these compounds form large ranges of homogeneity being very suitable for measurements as a function of concentration.

Within a homogeneous range of a compound the change of the work function mainly depends on the electron density at the Fermi level, according to the relation:

$$\Phi = U_B - E_F \tag{1}$$

The surface potential U_B is influenced by the distance of the atoms at the surface and is changed strongly by a phase transition. Systematic investigations as a function of the composition therefore can give information about the free electron concentration, the Fermi energy and about structure changes of

these materials. The aim of investigations is to find materials within a wide range of composition which show a strong interaction between interstitial and metal atoms.

On the other hand, and this is just equally important, concentration dependent investigations make it possible to estimate the influence of impurities such as oxygen, carbon, and nitrogen. These impurities nearly always exist in a pure transition metal or compound because these materials have a strong affinity to the mentioned metalloid atoms.

Measurements of work function were made in the zirconium-oxygen and zirconium-carbon systems. These systems were chosen because their structures and bonding relations are well known. It is possible to extend the results of these investigations to other transition metal systems since their electrical properties can be related to the valence electron concentration. However, it is necessary to compare compounds of the same crystal structure.

The two modifications of the Zr-O solid solution are characterized by different interstitial positions of the metalloid atoms. In the body centered cubic ß-modification the oxygen atoms occupy the tetrahedral sites and in the hexagonal closest α-modification the octahedral sites. In a similar way carbon occupies in the Zr-C system either the tetrahedral sites of the ß-modification or the octahedral sites of the face centered cubic carbide structure. With respect to the different sizes of the interstitial sites it is to be supposed that the influence on the work function should be different.

The investigated samples were disks with a diameter of 15 mm and a height of 5 mm. They were prepared by powder metallurgical methods. After hot pressing they were annealed 24 hours for homogenization. The measurements of work function were accomplished by the method of Schottky-Richardson. The samples were located plane parallel to the anode and heated by elec-

tron bombardment (fig. 1).

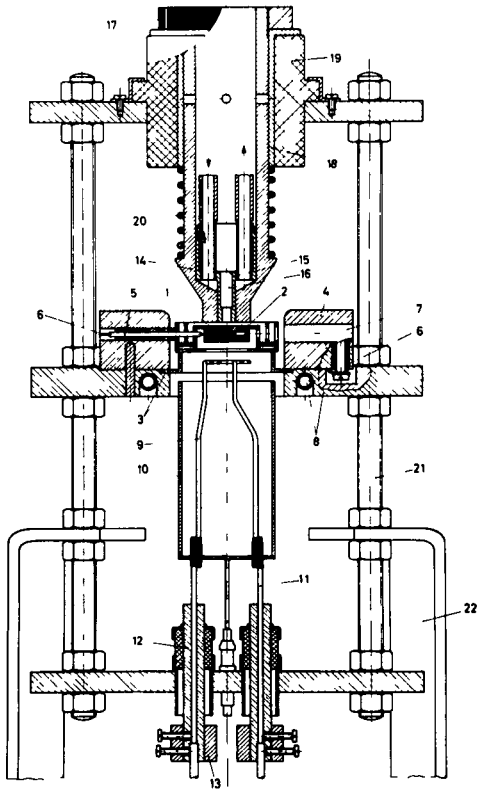

Abb 1 Aufbau zur Messung von Austrittsarbeiten

The temperature was measured at the surface by an automatic pyrometer. For this measurement the emissivity of the samples must be known. Before measurement the samples were annealed 4 or 6 hours at about 1700°C until constant measuring conditions existed. The tests were performed using a pulse technique. The acceleration voltage was put in shape of pulses which had a duration of about 1 ms, a height between 0.8 and 6 kV and a frequency of about 1 per second. The sample temperature gradually reduced during measurement and values of temperature, emission current and accelerating voltage were stored by an electronic short time sample and hold unit and then registered by a digital data acquisition unit. One result followed from about 2000 data points and was evaluated by a computer. It represents an average value over the different crystal directions and a mean temperature of about 1750°C.

The series of tests of the two Zr-O and Zr-C systems were carried out over large composition ranges. The sintered samples of the Zr-O system were chosen between 0 and 35 at-% and of the Zr-C system between 0 and 48 at-%. The phase diagrams of each system were used as the basis of the measurements.

In the zirconium-oxygen system the low temperature modification of the hexagonal α-phase extends from 0 to 31 at-% 0 (fig. 2)

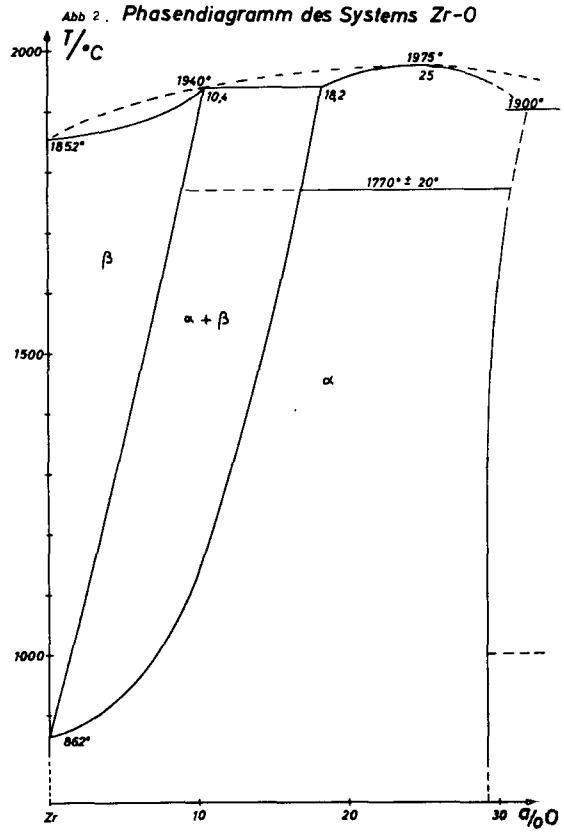

The body centered high temperature ß-modification is stabilized to 10.4 at-% 0 at 1940°C. At richer compositions ordered structures were found in the hexagonal solid solution which were reported in the literature. Recent neutron diffraction studies on α-Zr-O specimens quenched from 1300°C revealed an ordered arrangement of oxygen above 10 at-%. Below this concentration oxygen is randomly distributed on the interstices.

The measurements of work function indicate a strong interaction between interstitial and metal atoms. The measured work function curve (fig. 3) shows a very exact congruence with the phase diagram.

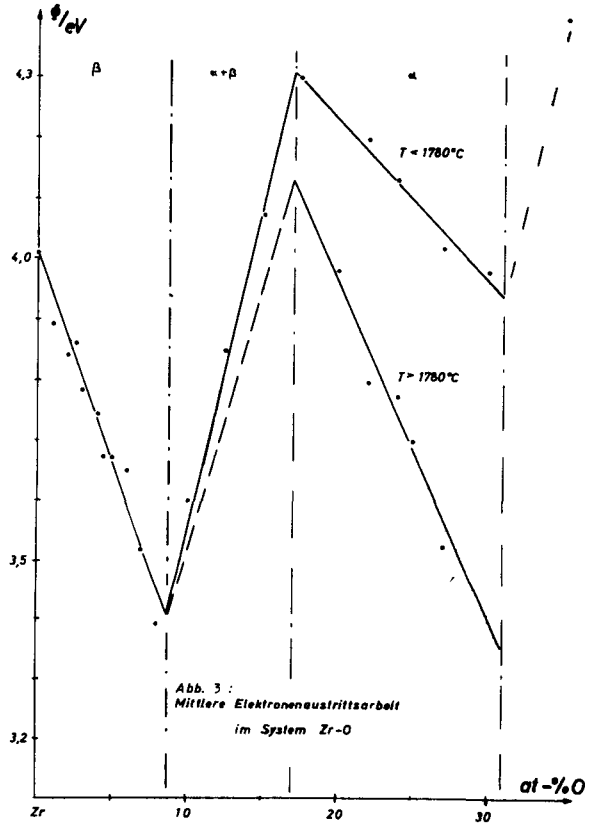

Abb. 3 :
Mittlere Elektronenaustrittsarbeit
im System Zr-O

The breaks of the curve at 9 and 17 at-% O agree exactly with the phase boundaries at mean measuring temperature. In the body centered cubic ß-solid solution the curve of measuring descends linearly from 4.01 to 3.39 eV. The lattice expansion in this range leads to a negligible variation of the surface potential of 0.2 %. According to eq. 1 the decrease of the work function is therefore brought about by the increase of the Fermi energy which is associated with an increase of the number of charge carriers in the metallic conduction band. The free electron model predicts that each oxygen atom will contribute 2 electrons to the increase of the charge carrier concentration.

The ionization of oxygen is improbable because of its great electronegativy. One must suppose that the energy bands of

metal and interstitial atoms overlap strongly. This may result from the fact that oxygen is by about 24 % larger than the theoretical size of the tetrahedral sites in a body centered cubic lattice, so that strong interactions occur between lattice and enclosed atoms. The strong bonding of oxygen in zirconium also results from the stabilization of the lattice by the interstitial atoms. This bonding is so stable that oxygen does not even evaporate when the compound is melted.

In the hexagonal α-composition the work function decreases from 4.31 to 3.94 or to 3.35 eV. The work function diagram reveals here a splitting into two sections, where the section with higher work function exists at temperatures below 1780°C and vice versa. In this range the Richardson line shows a break. The splitting could be explained by the existence of an ordered structure which turns in a disordered state, i.e. a random distribution, at temperatures above 1780°C. High temperature DTA analyses however have to prove this interpretation.

The transition from the ß- to the α-phase conforms with a structure change from a close to a closest packing. Thereby the diminution of the atom distances effects an increasing of the surface potential by about 6 % or 0.5 eV. Furthermore the octahedral sites in the hexagonal lattice have the larger size. The radii are 15 % larger than those of the oxygen atoms. Therefore the contribution to the conduction band diminishes in case of closest packing. The total result is that in the heterogeneous composition the work function increases with increasing concentration of oxygen.

Much greater changes occur in the zirconium-carbon system (fig. 4). Contrary to the Zr-O system carbon reveals only a very small range of solubility of about 0.3 at-%. However, a wide range of the face centered cubic carbide structure is found between 38 and 49.5 at-% C. In the lower sector of this carbide composition, neutron diffraction patterns revealed superstructure effects showing an ordered arrangement of the carbon atoms.

In analogy to the small solubility of carbon the work function curve (fig. 5) first decreases steeply to 3.38 eV and turns to an increasing behavior already at 0.3 at-% C.

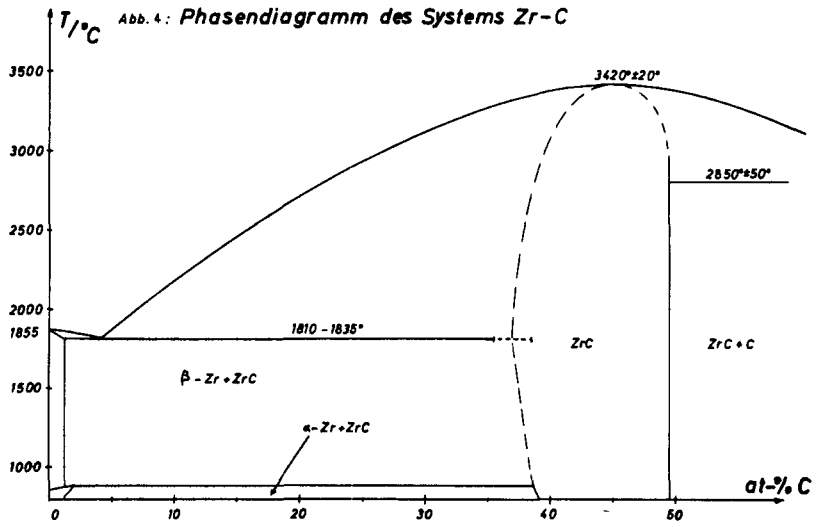

Abb. 4.: *Phasendiagramm des Systems Zr-C*

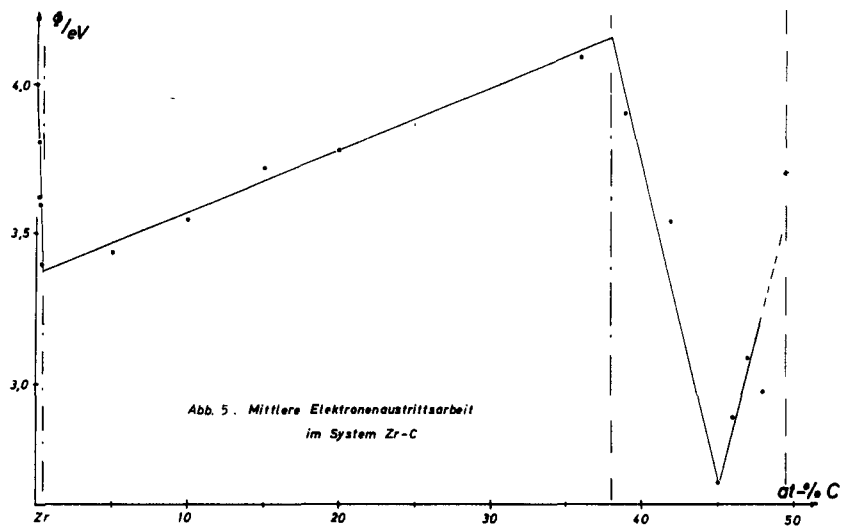

Abb. 5. *Mittlere Elektronenaustrittsarbeit im System Zr-C*

In the homogeneous cubic carbide range the work function changes from 4.15 to 2.67 eV. Here the break point at 45 at-% C indicates an ordered structure. In the heterogeneous range a linear transition is found between the measured results at the phase boundaries where the increase of work function also can be explained by the change from a close to a closest packing.

Compared to oxygen the carbon atom is about 28 % larger. This explains the extremely small solubility and also the steep decrease of work function of 0.62 eV within the very small composition interval of only 0.3 at-% C. The solubility of carbon is also very small in the other transition metal systems, for instance in the Ta-C system below 1 at-%, in the W-C system nearly nothing. The smaller the solubility, the stronger however are the effects one can assume according to the electron theory of the compounds. This fact is important, too, for assessing the influence of impurities, especially for the materials used in thermionic converters.

Owing to the stronger interaction of the carbon, its influence on the work function is more striking. The minimum of 2.67 eV at 45 at-% C also is of interest as it represents a total change of the work function in the Zr-C system of about 1.5 eV. These large differences make concentration dependent measurements very promising in seeking suitable thermionic converter materials.

High Work Function Dispenser Cathodes

E. Preuß

Institut für Technische Physik der Kernforschungsanlage
Jülich GmbH, Germany

The objective of these investigations is to develop dispenser cathodes with a high bare work function for operation at elevated temperatures in cesium filled nuclear thermionic cells. That means the work function should be not lower than 5.3 eV and the evaporation rate should be smaller than $9.7 \times 10^{-9} g/cm^2$ at a temperature of about $2000^{\circ}K$. This evaporation rate corresponds e. g. to a condensed layer of 0.15 mm of platinum on the anode within one year. Following the theory of Rasor, Warner and others a thermionic efficiency of about 17 % could be expected with such an emitter in the arc mode.

Generally these dispenser cathodes are composed of two materials, one of which is called the matrix material. It has a high melting point. The second one, which is called the additive material, has a low melting point but a high bare work function. The concentrations of these additive materials were in the range of 1 - 30 at. %. In most cases this concentration was 20 at. %. These additive materials were expected to diffuse to the surface and form a monolayer in order to get a higher work function than it would be possible with the matrix material only. A second additive material e. g. cerium in the concentration of 2.5 at. % was added to get a better wetting of the surface by the high work function material. As it turned out this second additive material did not improve the high work functions.

There are two considerations which governed the selection of these materials. Firstly they must have a small tendency of

forming alloys at high temperatures. Secondly they must have a low absorption cross section for thermal neutrons since it is desired that the emitters be usable in a moderated nuclear reactor. The latter could also be achieved by coating emitter bodies of molybdenum by thin layers of those high work function emitter materials.

These considerations led to the selection of the materials in table I.

Preßsintermaterial			max. Elektonenaustritts-arbeit mit Pt [eV]
Matrix	1. Zusatz 1-20 At.%	2. Zusatz 1-2,5 At.%	
W	Pt oder Os	Ce	5,35 (1900 °C)
Re			4,78 (1733 °C)
Mo			4,51 (1878 °C)
ZrC			4,30 (2010 °C)
TaB_2			3,50 (2000 °C)

Table I

The matrix materials were the refractories W, Re, Mo, ZrC, and T_aB_2. The additive materials were Pt or Os with the second additive material Ce. Molybdenum had the lowest melting point of those matrix materials. It was only used because of its small cross section for thermal neutrons. In combination with platinum it failed as a high work function material because it formed an alloy at low temperatures. On the right side of this table are listed the highest work functions and the corresponding temperatures which were measured for platinum and cerium as additive materials. The work function of the samples with osmium as additive material have not yet been measured.

The starting materials of the samples were in the form of powders. The specimens were fabricated by hot pressing at a temperature of 1400°C and a pressure 200 kp/cm^2. This was done in an argon atmosphere. Subsequently the specimens were degassed at 1700°C for at least 24 hours in high vacuum. The diameter of the specimens was 8 mm and the height was 2 mm.

Fig. 1 shows a schematic drawing of the experimental set up.

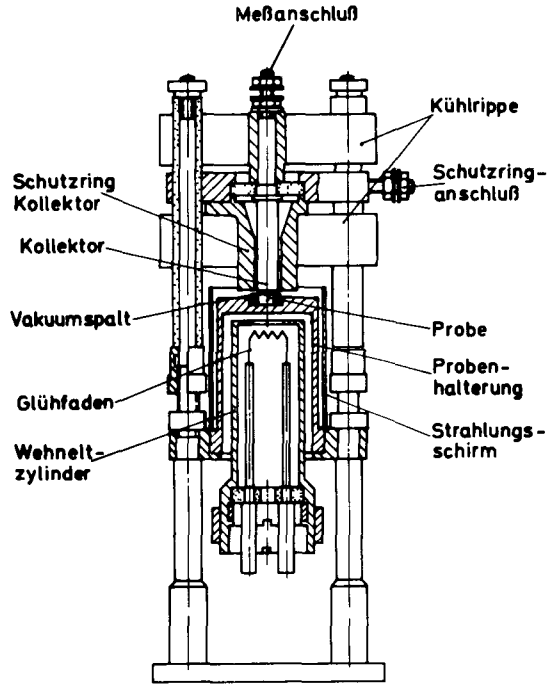

Fig. 1 Schematic drawing of the experimental set up for work function measurements in high vacuum

The lower part shows the electron gun used to heat the assemblies and in the upper part can be seen the guard ring-collector assembly used to measure the emission current of the specimens. The temperature of the samples was measured pyrometrically. In some specimens small holes were bored in order to get the black body temperature since the emission coefficients of those materials were unknown. The work functions were calculated from the measurement of the saturation currents by the use of the Richardson equation.

Fig. 2 through 5 show the work function of tungsten with the platinum additive as a function of temperature.

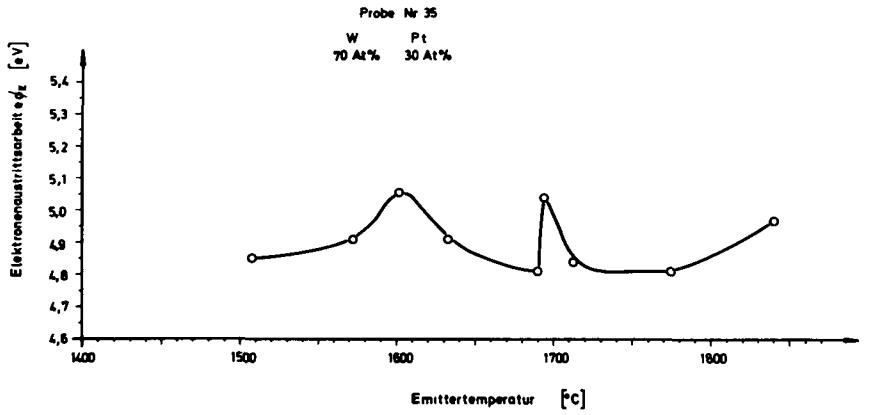

Fig. 2 The work function of a W-Pt sample as a function of temperature

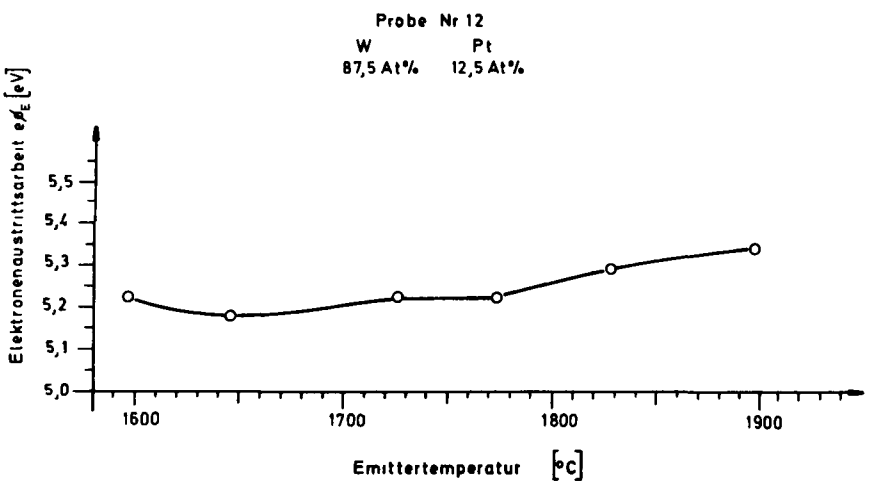

Fig. 3 The work function of a W-Pt sample as a function of temperature

In the case of 30 at. % Pt a rise in the work function near the melting point of platinum was observed. The work function was about 5.1 eV. When the concentration of Pt was lowered to 12.5 at. % the work function of 5.35 eV was measured at a temperature of about 1900°C. The surface of this specimen was polished in contrast to the surfaces of the other samples. With a lower concentration of platinum the work function decreases. This is demonstrated in fig. 4 and 5 where the concentration of platinum is 5 at. % and 1 at. % and the corresponding work functions are 5.15 eV and 4.7 eV respectively.

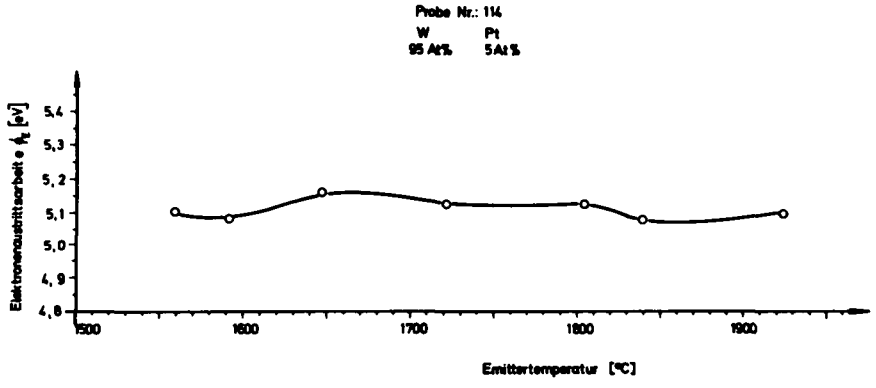

Fig. 4 The work function of a W-Pt sample as a function of temperature

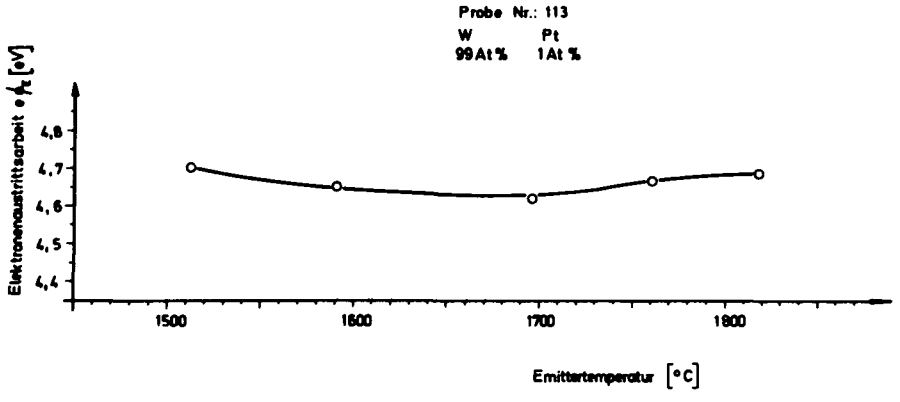

Fig. 5 The workfunction of a W-Pt sample as a function of temperature

As already mentioned the addition of cerium as a second additive material did not yield a high work function. This is shown in fig. 6.

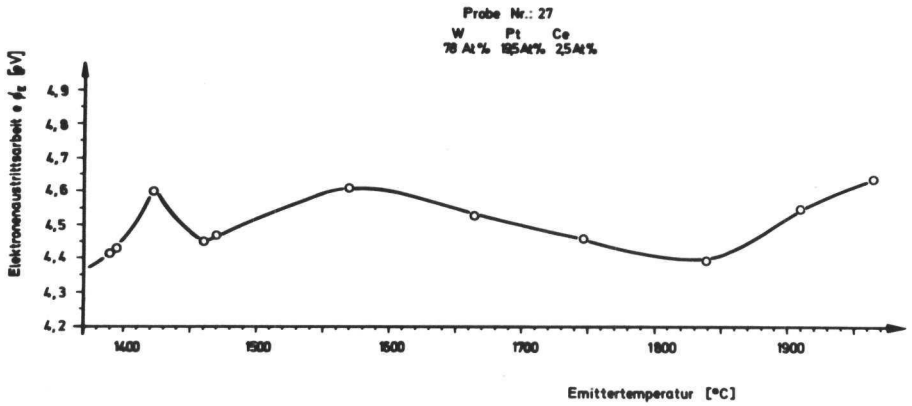

Fig. 6 The work function of a W-Pt-Ce sample as a function of temperature

A cross section of the sample containing 20 at. % Pt is shown in fig. 7.

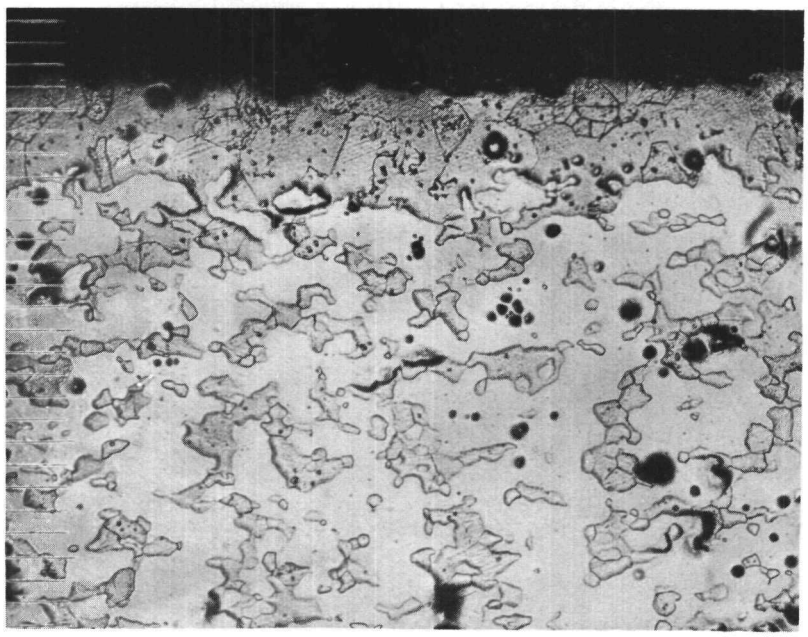

Fig. 7 Cross section of a W-Pt sample taken by light microscope

There are two phases to be seen, a bright and a gray one. At the surface of the sample a layer of about 20 μ thickness is formed by the gray phase, which is desirable from a standpoint of allowing for better diffusion of the additive material. Fig. 8 is an X-ray picture of this cross section taken by an electron microprobe.

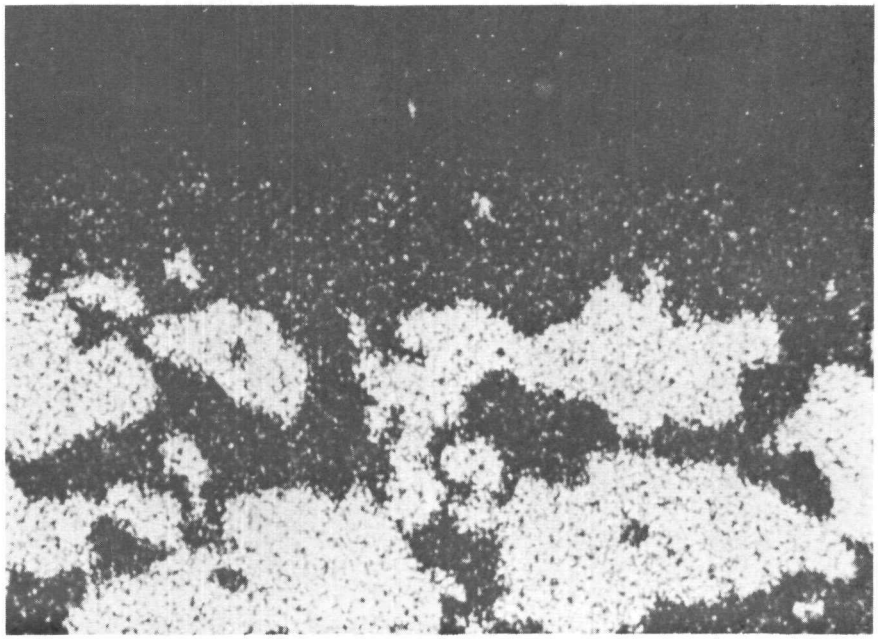

Fig. 8 Cross section of W-Pt sample taken by electron microprobe

The bright zones are an alloy of 60 at. % Pt and 40 at. % W. The dark regions are pure tungsten. Thus the surface layer of the sample appears to be tungsten. No platinum could be detected by the electron microprobe at the surface of the sample. Before this metallographic investigation the sample was kept for several hours at a temperature of about 2100°C.

A line scanning from this cross section is shown in fig. 9. Here the X-ray intensities measured by the electron microprobe for W, Pt, O, and Na are plotted on an arbitrary scale as a function of the distance from the surface. In the alloy formed of platinum and tungsten, traces of oxygen could be detected. Since the ion currents of this specimen were rather high it was suspected that these currents were formed by impurities

like sodium or similar elements from the sample. But as the line scannings demonstrate sodium could not be detected.

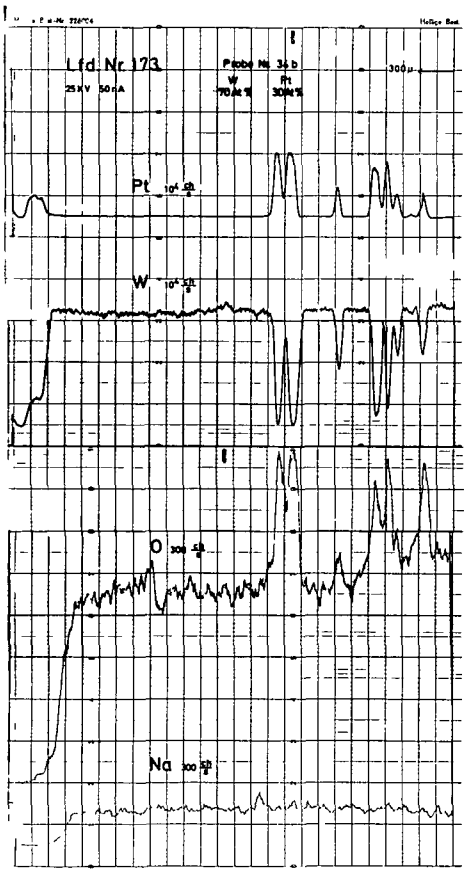

Fig. 9 Line scannings of Pt, W, O and Na in the surface of the W-Pt sample

The distribution of the work function on the surface of a sample containing 20 at. % Pt was observed by Alleau at the Centre d'Etudes Nucléaires de Saclay with an electron emission microscope. Fig. 10 shows a picture of this surface obtained by this technique. The diameter of the circle is about 0.5 mm. The temperature of the sample was about 2000°C and the vacuum $2 \cdot 10^{-7}$ torr. From this picture it can be seen that the distribution of the work function at the surface is rather homogeneous. The curve of this distribution was traced electronically with the result shown in fig. 11.

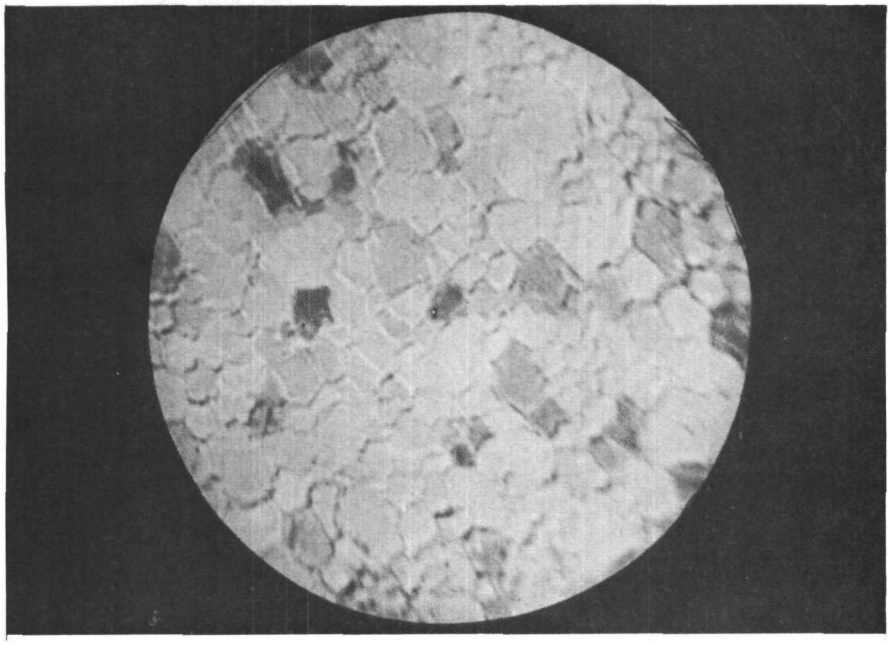

Fig. 10 The surface of a W-Pt sample obtained by an electron emission microscope

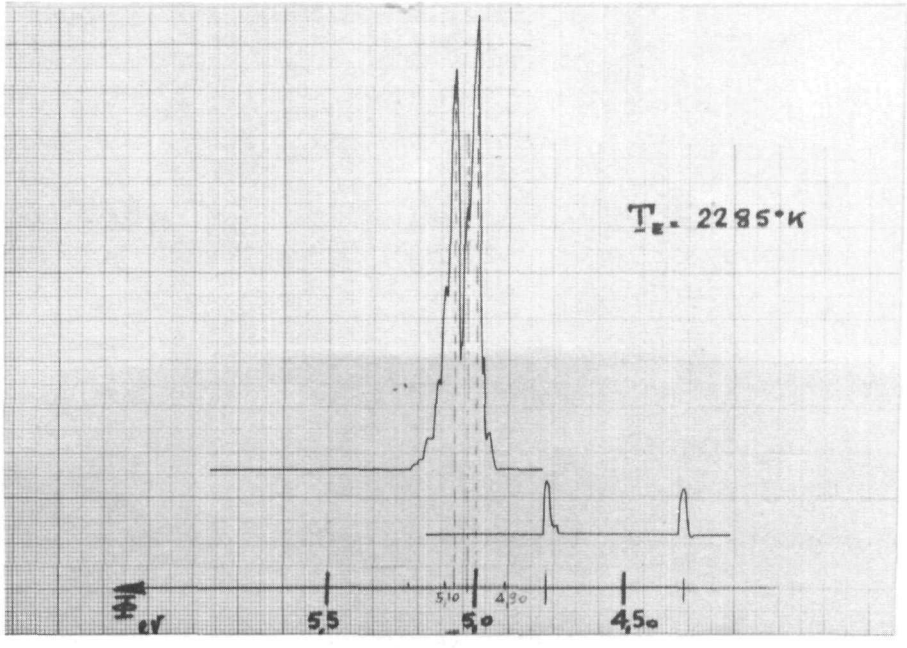

Fig. 11 Work function of a W-Pt sample distribution

The height of this curve is proportional to the amount of the surface area having the corresponding work function given by the abscissa. There are two **peaks** at 5 and 5.1 eV resp. The mean work function was estimated to be 5.05 ± 0.05 eV which corresponds very well with the work functions calculated from our measurements of the saturation currents.

The evaporation rate of platinum from such a sample of tungsten containing 20 at. % Pt was measured by Butz. Fig. 12 shows schematically the experimental arrangement

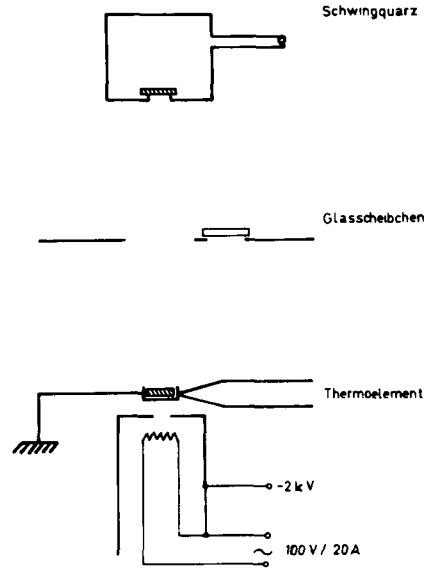

Fig. 12 Schematic drawing of the experimental arrangement for the measurement of the evaporation rate.

The sample was heated by an electron gun in high vacuum ($< 10^{-6}$ torr). The temperature of the sample was measured by a thermocouple. The platinum which was evaporated condensed on the crystal of a quartz balance. By this means the relative

amount of platinum evaporating from the specimen as a function of time could be measured (see fig. 13).

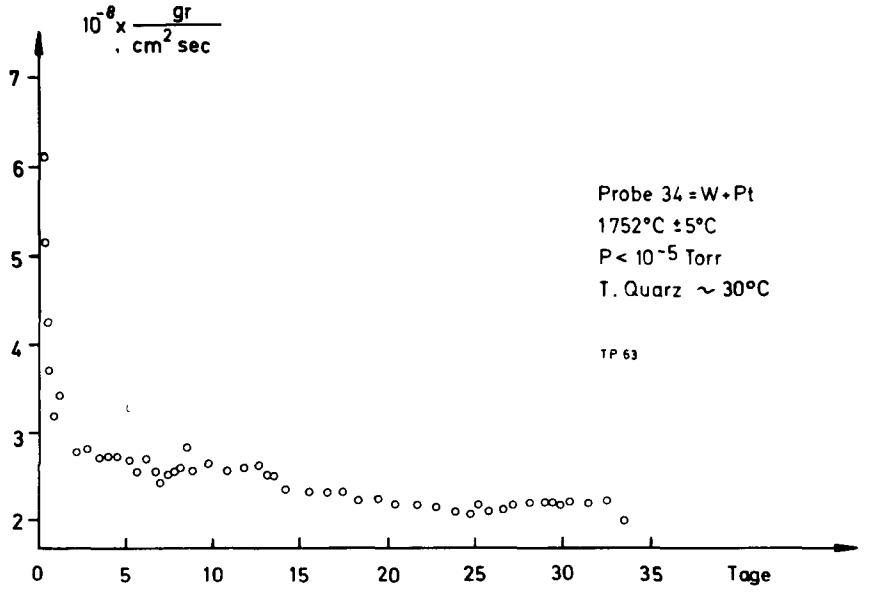

Fig. 13 Evaporation rate of Pt from a W-Pt sample

The sample was kept at a temperature near the melting point of platinum. Beneath the quartz crystal there was a glass disk on which the platinum also condensed. Electron microprobe measurements of the X-ray intensity from the platinum of this layer were compared with intensity measurements for condensed layers whose thickness had been determined by differential weighing. In this way the calibration of the ordinate in fig.13 was obtained. After several days of heating a constant evaporation rate of about 2×10^{-8} g/cm^{2}s of platinum was measured. By this method of calibration with the electron microprobe the small amounts of tantalum and tungsten which evaporated from the support of the specimen and from the matrix of the specimen itself could be eliminated.

Our work function measurements with the other materials such as ZrC-Pt-Ce and Re-Pt-Ce are traced in fig. 14 and 15.

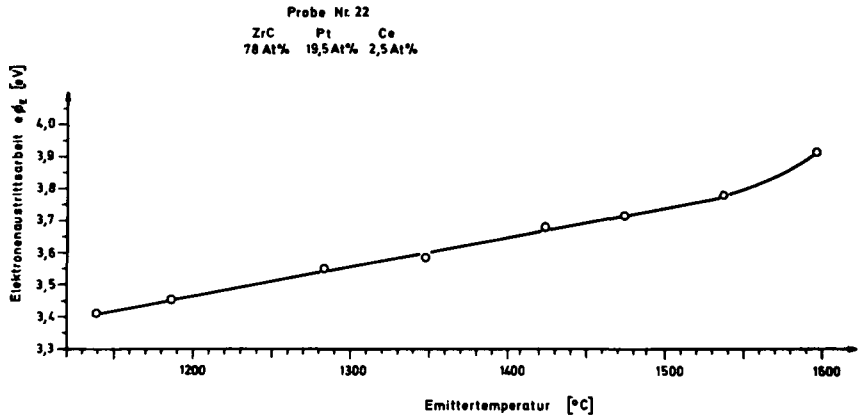

Fig. 14 The work function of a ZrC-Pt-Ce sample as a function of temperature

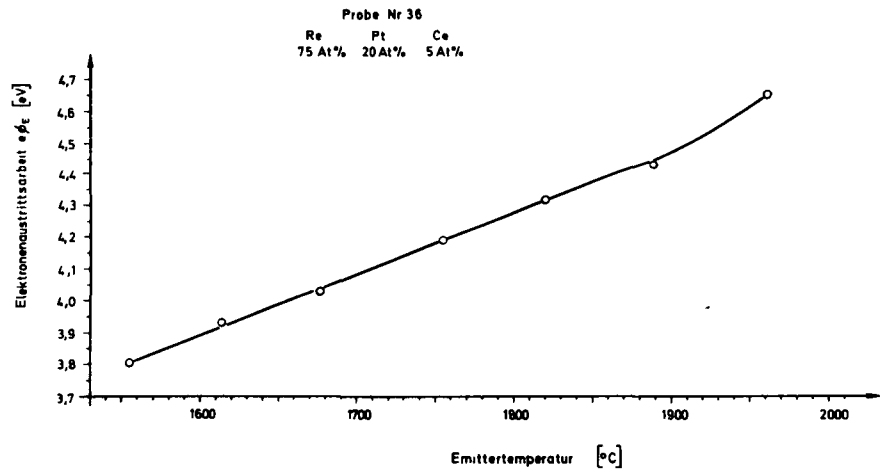

Fig. 15 The work function of a Re-Pt-Ce sample as a function of temperature

Both materials showed an increase in work function at elevated temperatures. But generally the work functions were smaller than those of the tungsten-platinum samples. Therefore these materials are not so efficient as thermionic emitters as e. g. the dispenser cathodes of the tungsten-platinum type.

Finally some remarks should be made about the feasibility of pressing thin layers of dispenser type emitter materials on stems of molybdenum. Pidd et al.[1] describe a method for hot pressing 0.5 mm thick UC-ZrC layers on stems of tantalum. Several different shapes of the support stems were tested as seen in fig. 16.

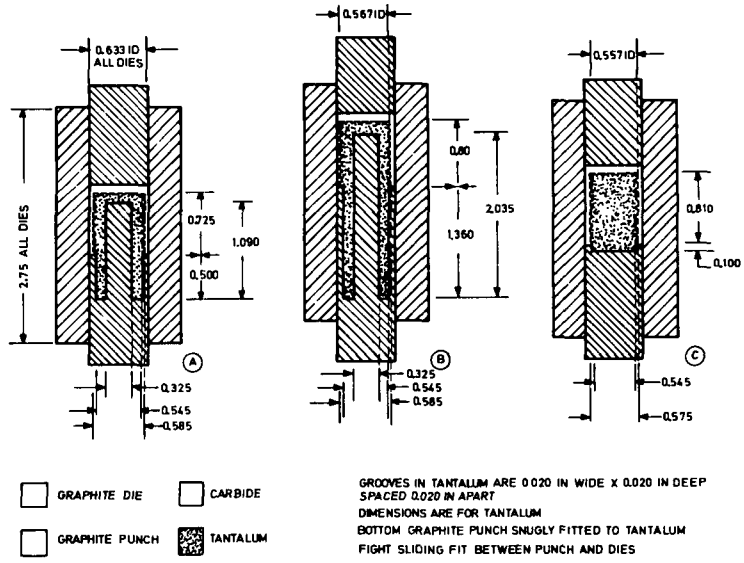

Fig. 16 The arrangement for hot pressing carbide to tantalum sleeve after Pidd at al.[1]

The experimental arrangement for the hot pressing process is drawn up schemtically. By this methode a most convenient shape for the tantalum stem could be selected. This might be a chance that a similar approach for the fabrication of high work function dispenser cathodes may be achieved. Perhaps diffusion barriers between the support stem and the thin emitter layer may be used as in the case of vapor deposited layers. But the advantage of the high work function dispenser cathodes is that the bare high work functions of the emitter and collector sur-

faces are steadity replenished. In this manner the possible negative influence on work function of some fission products which diffuse onto the surfaces, might be eliminated.

(1) A.E. Campbell, F.D. Carpenter, I.B. Dunlay, and R.W. Pidd, AD 284 410

Fabrication of Cermet Electrodes

D. Schmidt

DFVLR - Institut für Energiewandlung und elektrische Antriebe, Stuttgart - Vaihingen, Germany

From bibliographical data and our own measurements the following results can be shown:

If the operating temperature of cermet electrodes with variable density and constant chemical composition is chosen such that the permissible maximum evaporation rate is just reached, then one has to except that the emission current of such electrodes which exhibit the highest density, is also higher.

In order to examine this influence of structure and density on the emission properties and other properties of such electrodes a method to fabricate them was developed and tested. From the point of view that the distribution of the ceramic component in the matrix should be very uniform, it appeared that powder metallurgical processes are in general preferable to melting methodes. The structure and density of the electrodes may be changed by varying the properties of the basic powders and by altering the method of densification.

We chose the system barium-calcium-tungstate-tungsten and first changed the properties of the metallic component tungsten (fig. 1). In fig. 1 the decrease of the mean particle size of tungsten from column 5 to 3 leads to an increase of the filling density and the density of the compact densified by vibration. The particle size distribution of the different powders was measured by sedimentation of the powder out of a suspension. Using Stoke's law a correlation between the increasing weight on the balance as a function of time and the

particle size could be found (fig. 2a and fig. 2b).

Powder Material	Ba_2CaWO_6	W (HC 300)	W (HC 200)	W (HC 30)
Purity : %	99	99,95	99,87	99,87
Theoretical Density (TD) : g/cm^3	7,03	19,3	19,3	19,3
Filling Volume : $\frac{cm^3}{100g}$	56,5	26,7	28,1	114
Filling Density : $\frac{g}{cm^3}$	1,77	3,75	3,56	0,877
(% TD)	25,3	19,4	18,4	4,5
Vibrated Volume : $\frac{cm^3}{100g}$	43,0	18,75	19,66	84
Vibrated Density : $\frac{g}{cm^3}$	2,32	5,32	5,09	1,19
(% TD)	33,3	27,5	26,2	6,2

Fig. 1 Characteristic datas of the powders

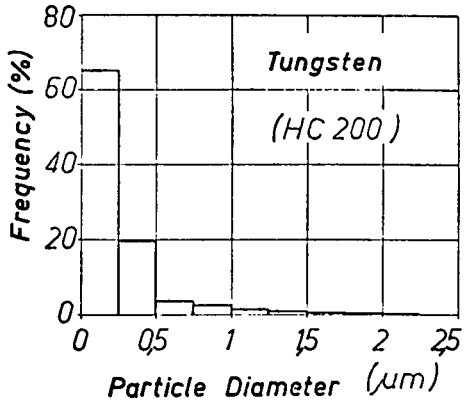

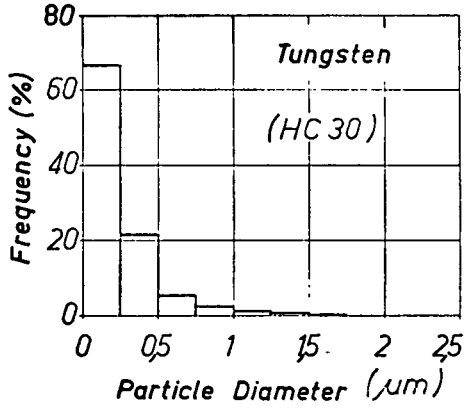

Fig. 2a Distribution of particle diameters

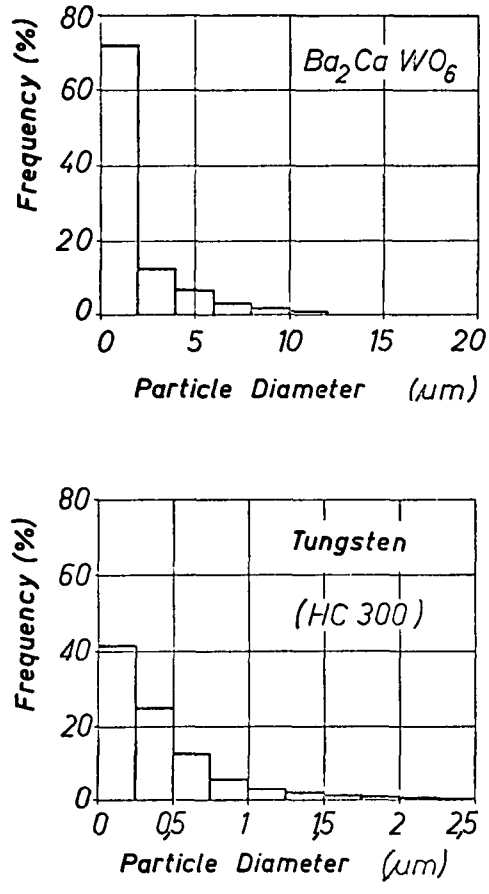

Fig. 2b Distribution of particle diameters

This method is not good enough for very small particle sizes for it is rather difficult to get a good suspension of such powders i. e. to destroy the agglomerates. The difference between the two finest powders is to be seen in x-rays. Regarding the intensity of the lines it is to be seen that the bottoms of the lines are broadened with decreasing particle size of the powders (fig. 3).

Mixing of the ceramic component barium-calcium-tungstate with each of the different tungsten powders was succesfully accomplished by dry mixing for a long time. The powder had been first dried by heating in a high vacuum and then tumbled in a container. The relation of container volume to powder volume was about 3, the tumbler movement 50 rotations per minute. After about a 100 h the shape of the x-ray lines from $Ba_2\,CaWO_6$ and W coincided. The mixtures gained a high degree of homogenization. Preliminary tests to mix the

powders in a suspension gave poor results because the two electrode components exhibited a high difference in specific gravity. This led to a segregation of the powders in the course of the drying process.

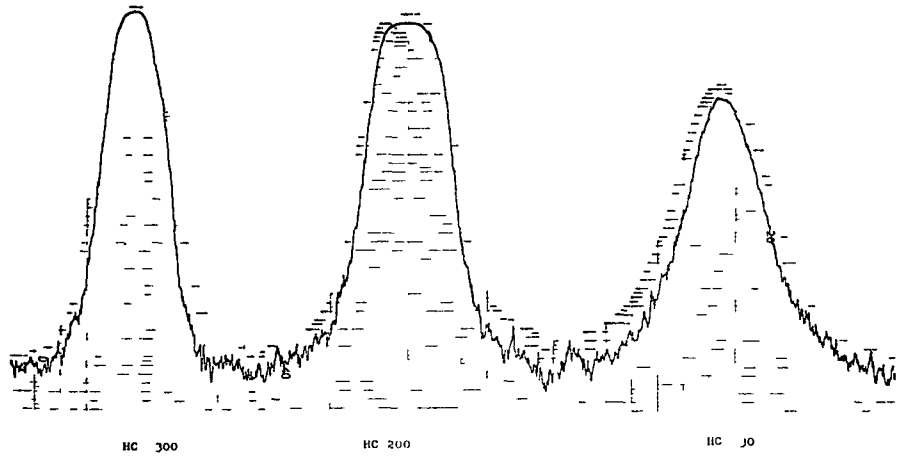

Fig. 3 Intensity distribution of lines of different W-powders

In order to make a survey of the sinterability of the different mixtures, pellets were cold pressed in a double ended press with stearin lubricated dies. The compacting pressure was 10 Mp/cm^2. When heating these pellets in a dilatometer the linear shrinkage as a function of the increasing temperature ($5^{\circ}C$/min) could be recorded (fig. 4). In the medium range the expansion and the shrinkage are superimposed, until above a certain temperature the shrinkage becomes dominant. The temperature of the beginning of the shrinkage is defined as that where 0.2 % shrinkage has taken place. Another method to determine the beginning of sintering was to measure the electrical conductivity as a function of the increasing temperature (fig. 5). It proved to be of special interest for compositions with high ceramic content.

Cold compacting of pellets and sintering without pressure led to high differences of the density in the same pellet. Cracks, internal stresses and different emission current density for different pieces of the same pellets were observed. These

faults were avoided by the combination of the sintering and pressing treatments by hotpressing.

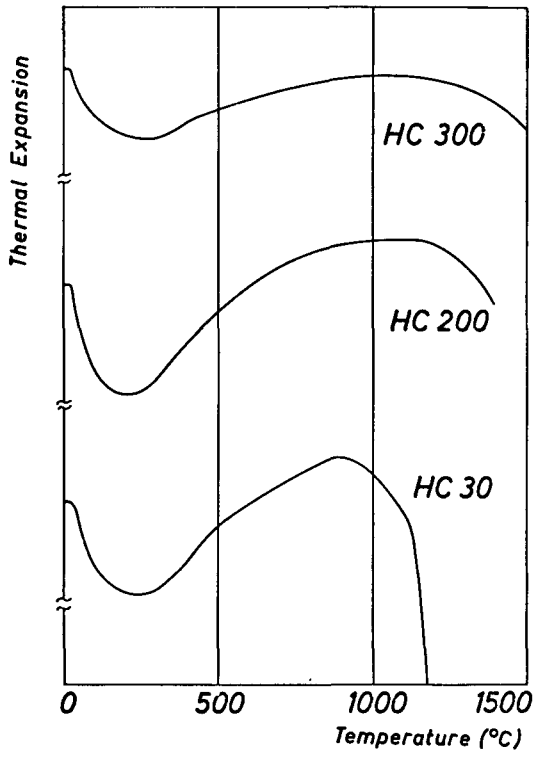

Fig. 4 Thermal expansion of pressed tungsten specimens

The common die material graphite could not be used, for the ceramic electrode reacted with it. X-ray examination showed carbon in the inner part of the pellet. Heating alumina in contact with the electrode material let to better results. At the border of the metallic component tungsten, no reaction zone could be detected, and at the border of the ceramic component only a thin reaction zone could be distinguished, which could be easily removed. In the die we used for the densification of our electrode material (fig. 6). A tube of alumina can be seen. This tube has to be changed for each pellet. It is fitted in another tube of molybdenum. The plugs of alumina are supported by graphite, which also suscepts the heating energy. This latter was induced by a high frequency coil. In the course of the hotpressing process the electrode material

was first slowly heated under a small pressure, so that rest of gas could be easily pumped in order that the pressure in the system would not increase.

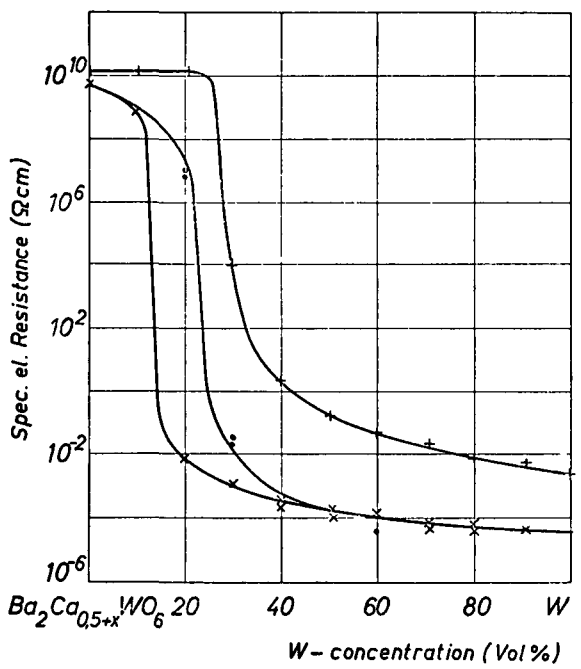

Fig. 5 Specific el. resistance of $Ba_2Ca_{0.5+x}WO_6$-W specimens as function of W- content

pressed specimens +
presintered specimens o 2 h 1260°C
x 14 h 1260°C

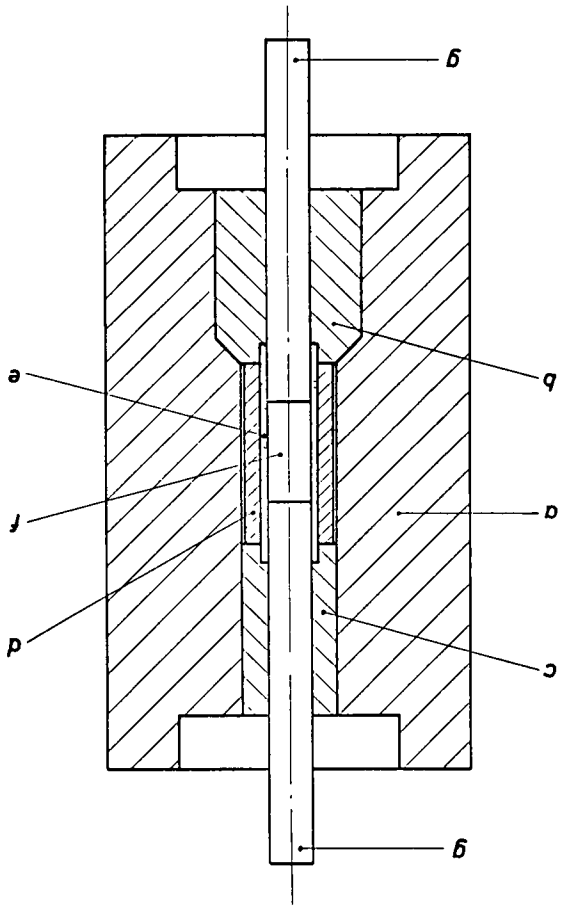

Fig. 6 Die for hot pressing

a,b,c)	graphite	d) molybdenum
e,g)	alumina	f) electrode material

When the temperature at which sintering began to place was reached, the full load was introduced. The support of the two plugs was designed in such a manner that the full load could be held constant for the whole time of sintering. The linear shrinkage of the pellets was recorded by the movement of the two plugs (fig. 7). The main part of densification was soon finished (~30 min.). The final density of the sintered bodies could be adjusted by the pressure and temperature in the hot-pressing process.

Thin discs of the electrode material usually have to be fixed to a support in order to measure the emission properties. By electron beam welding we succeeded in joining the brittle electrode material to a molybdenum support. The direct pene-

tration of the electron beam into the cermet electrode was disadvantageous. All trials led to a cleavage of the electrode material (fig. 8).

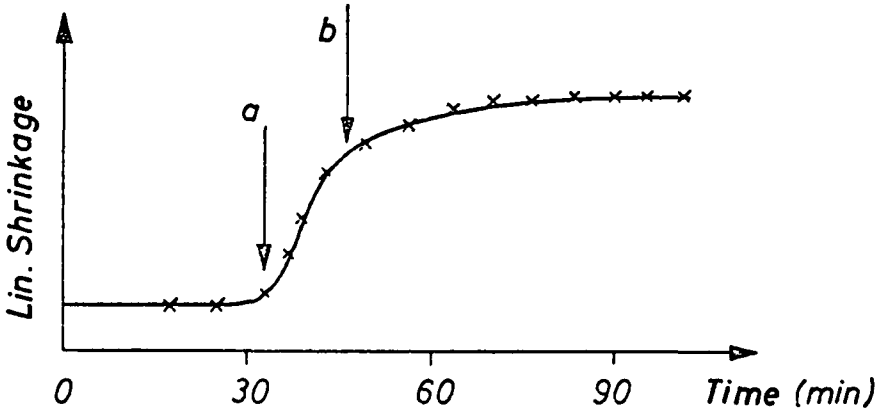

Fig. 7 Linear shrinkage of the electrode material during the hot pressing process

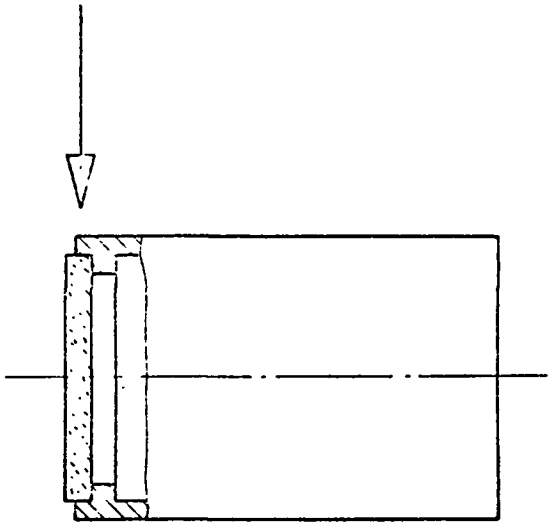

welding method I

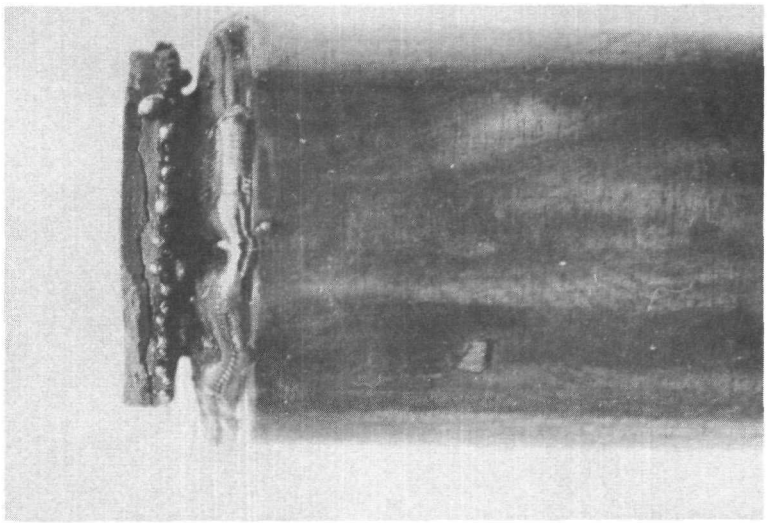

Fig. 8 Transition cermet electrode - support

Evaporating parts damaged the lower part of the weld, so that on this part of the weld only spots of a tolerable weld remained. Good connections could be obtained by directing the electron beam parallel to the axis of the cermet electrode into a thin ring of the molybdenum support (fig. 9).

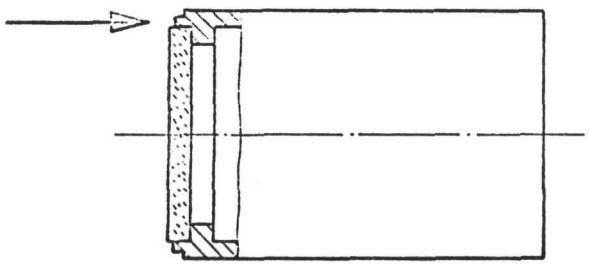

welding method II

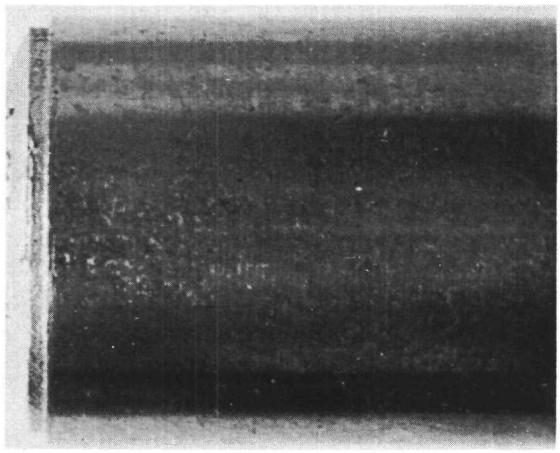

Fig. 9 Transition cermet electrode - support

The microphotograph of a section of such a vacuum tight welding zone shows how the relatively large grains border on the small grains of the cermet electrode (fig. 10).

cermet electrode

molybdenum support

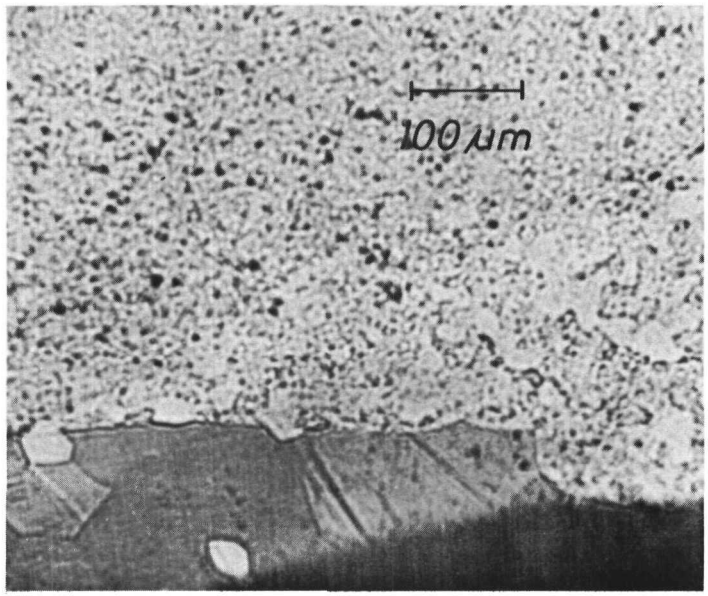

Fig. 10 Microphotograph of the transition zone

Measurements of the Work Function of Surfaces with Adsorbed Layers without Electron Emission of the Sample

M. von Bradke

DFVLR - Institut für Energiewandlung und elektrische Antriebe, Stuttgart - Vaihingen, Germany

A brief review is given about the presently known methods for work function measurements on surfaces with adsorbed layers and about their working range. Furthermore an improved Shelton-method is described, which allows the extension of the measurements to the low temperature and low pressure range. The magnetic focusing of the electrons in the original Shelton-divice is replaced by an elektrostatic focusing; an enclosed space is formed by the anode, the accelerating electrode and an insulating ceramic ring. Thus any influence of the adsorbing vapor on the work function of the cathode can be avoided. A technological description is given for the most important parts of the measuring system. Finally some test measurements of high vacuum work function are reported.

Introduction

Measurements of work function have been carried out on electrodes with adsorbed layers of cesium because of the particular interest in such electrodes having an especially low work function. The first measurements made on electrodes with adsorbed layers of cesium were carried out by Taylor and Langmuir[1]. Their measuring method was suitable for the range of high electrode temperatures and low pressures. A first improvement of the measuring range was obtained by the plasma immersion technique, developed by Marchuk[2] and employed extensively by Houston[3]. This method extends the measuring range to high vapor pressures.

Fig. 1 gives a rough summary for the range of application of these methods.

	Low Vapor Pressure	High Vapor Pressure
High Temperature	Taylor , Langmuir Method	Marchuk – Houston Method
Low Temperature	Improved Shelton – Method	Extended Marchuk-Houston – Method

Fig. 1 Work function measuring methods and their working range

Both are applicable only for the range of high electrode temperatures. The reason is that in both cases the work function is determined by saturation emission, applying the Richardson equation. At low temperatures this method becomes more and more uncertain and finally impracticable.

The minimum work function for most adsorption systems is within this temperature range. Theories developed by Rasor and Warner[4], Gyftopoulos and Steiner[5], and by Luke and Smith[6] for the work function of electrodes with adsorbed layers deviate from each other in the range around work function minimum. Latest experimental results, as reported for instance by Müller in a preceding report, suggest that assumptions in these theories are not valid for high cesium coverages.

Last year at the Stresa conference a paper was presented by Bundschuh[7], which contained suggestions for the extension of the range of the plasma immersion technique to low temperatures. By this method the range of low electrode temperatures and high vapor pressures may be covered as shown in fig. 1. In our institute a method has been developed for the low temperature and low vapor pressure range. In the following this measuring method will be described and technological experiences concerning the design of the measuring device will be reported.

Measuring Method

The measuring technique was first applied by Shelton[8]. An accelerating electrode with a small hole is placed in the interelectrode gap of a plain parallel diode. A superposed longitudinal magnetic field focuses the emitted electrons and reproduces the aperture of the accelerating electrode on small patches of anode and cathode which can be examined locally by this method.

With a sufficiently high positive potential of the accelerating electrode, the emission current is not space charge limited. In the current-voltage characteristic the region of retarding potential borders directly on the region of saturation current. From the slope of retarding potential characteristic and from the height of saturation current, temperature and work function of the cathode can be determined. The work function of the anode can be calculated by subtracting contact potential between anode and cathode from work function of the cathode. The contact potential is given by the position of the current voltage characteristic along the voltage axis. At the transition point between retarding potential and saturation current the external voltage between anode and cathode is equal to the contact potential. A model of the corresponding potential distribution in the diode is shown in fig. 2a.

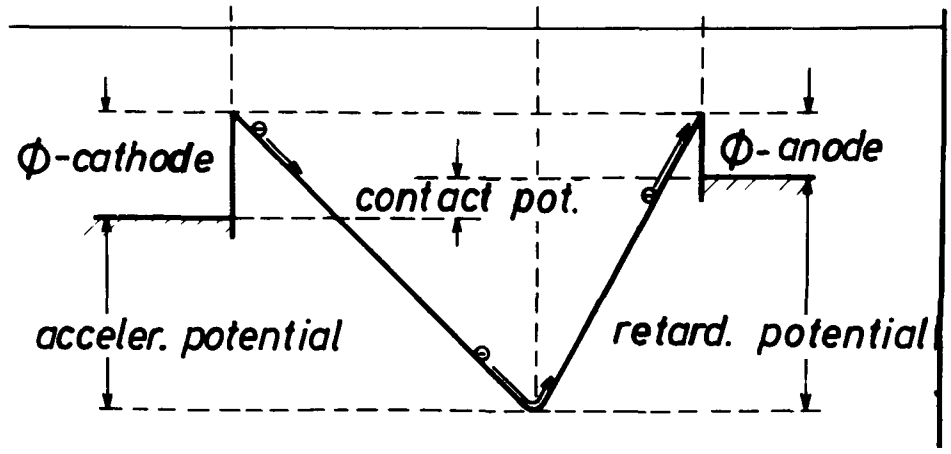

Fig. 2a Potential model

Batzies[9] measured by this method the work function of electrode materials in high vacuum and Kisliuk[10] on electrodes with adsorbed layers of nitrogen and oxygen.

For our requirements the original arrangement of Shelton was modified: Magnetic focusing of electrons was replaced by electrostatic focusing. An electron beam gun focuses the emitted electrons on the hole in the accelerating electrode. The accelerating electrode, the anode and an insulating ceramic ring between them form a closed space, containing the vapor of adsorption substance. Fig. 2b shows schematically this arrangement.

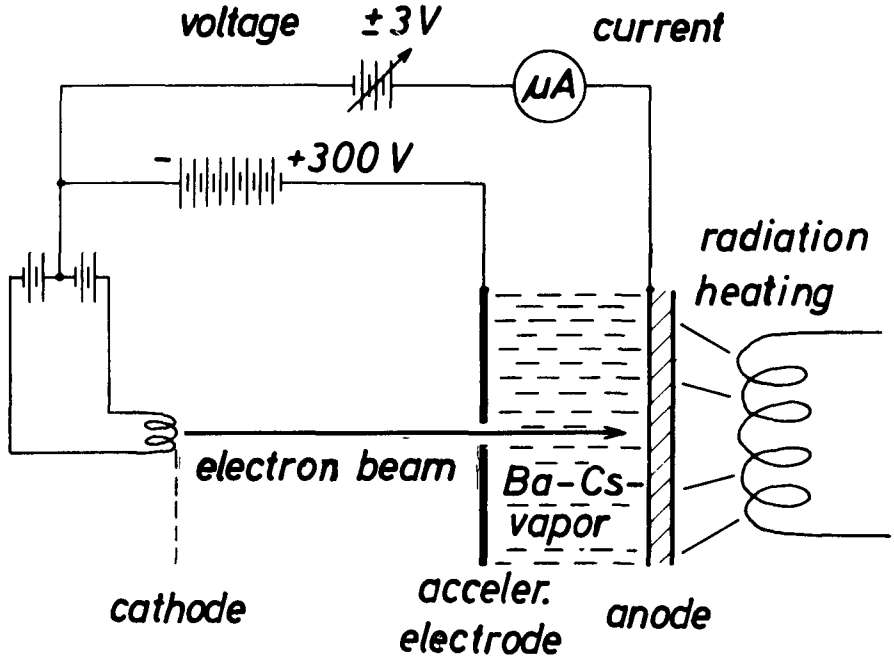

Fig. 2b Measuring device, schematically

The work function of the cathode is constant during the experiments because there is no influence of adsorbing vapor. Thus changes of work function of the anode cause equal changes of contact potential. These changes can be measured as a shift of the current voltage characteristic parallel to the voltage axis, as shown in fig. 3a.

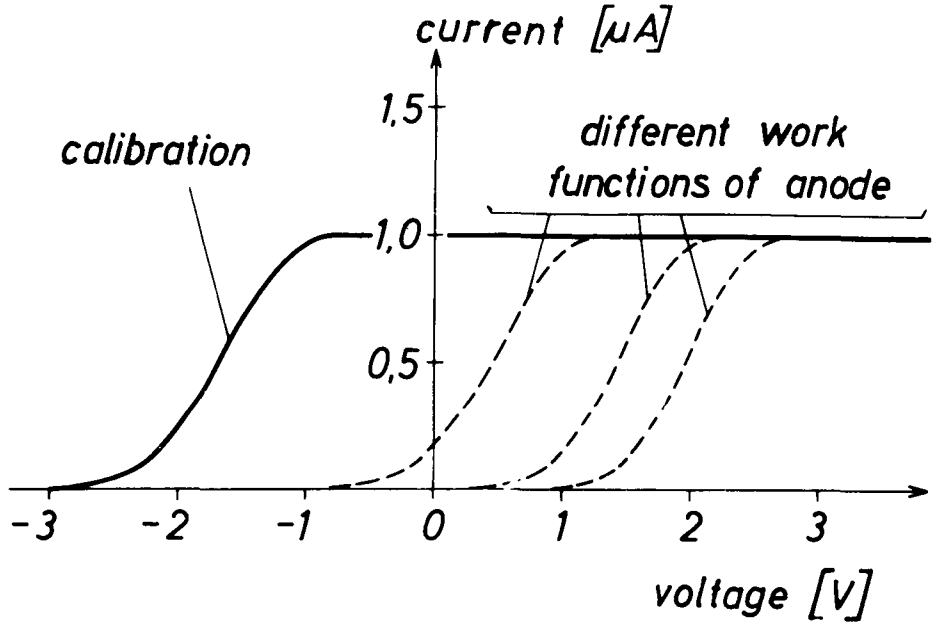

Fig. 3a Current voltage characteristic

It is possible to calibrate the device for measuring absolute work function values by comparing with measurements on single crystals in high vacuum.

For fast and vonvenient measurements the current voltage characteristic is displayed on an oscilloscope and can be recorded photographically. An example is given in fig. 3b.

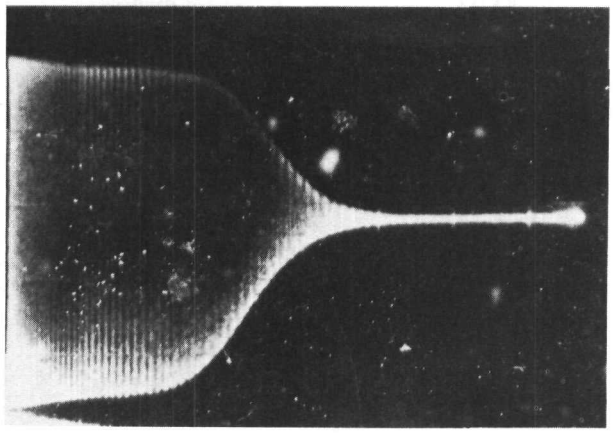

Fig. 3b Characteristic displayed on the oscilloscope

Measuring Device

Fig. 4 shows a sketch of the essential parts, the electron beam gun, the accelerating electrode and the anode , which is the investigated sample.

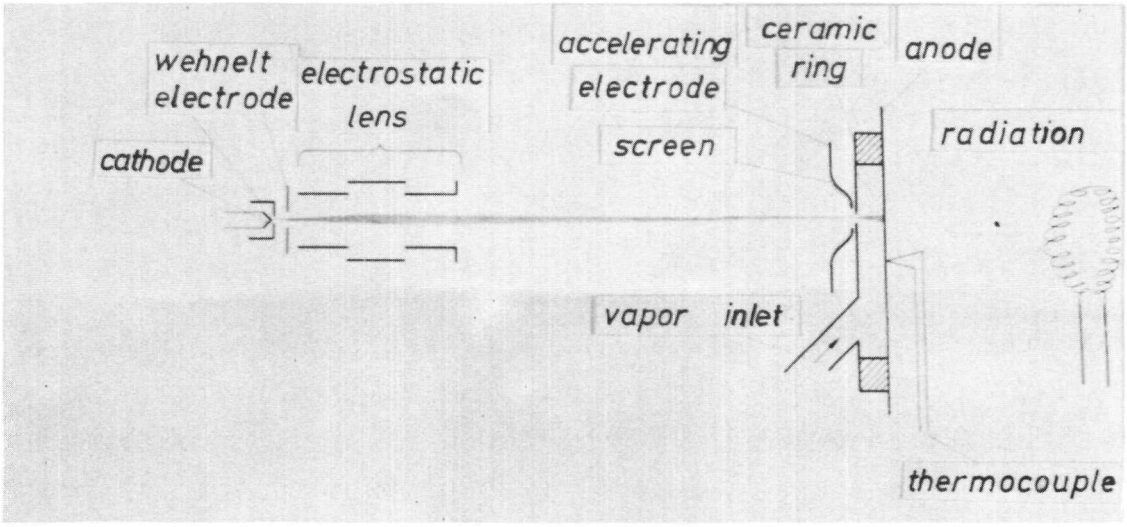

Fig. 4 Parts of the measuring system

The whole measuring device including the vapor supply system are enclosed by a vacuum vessel. The sample can be changed without opening the vessel. The vapor supply system consists of two evaporating containers connected in series. During

operation it is connected to the surrounding vacuum through a condensation trap. Thus the pressure of residual gases is low within the system.

All parts of the measuring system which are in direct contact with adsorption vapor are constructed of molybdenum and high purity alumina ceramic. These parts can be held at temperatures up to 1200°C continuously.

Work function measurements, especially in the low temperature range, are highly influenced by impurities from the residual gas pressure in the vacuum system. In the interesting temperature range this pressure has to be less than 10^{-10} torr to keep the sample free of contamination. The required ultra-high vacuum system is pumped by two mercury diffusion pumps with liquid nitrogen cold traps through a bakable valve and an additional Vac-Ion pump which is connected directly to the vacuum vessel. The whole ultra-high vacuum section of the system is bakable up to 450°C including the upper stage of the second diffusion pump. In this vacuum system residual gas pressures of the order of 10^{-12} torr have been obtained.

Conclusion

During initial tests of the measuring device, work function measurements on polycrystalline tungsten and tantalum were carried out in ultra-high vacuum. The difference of their work function was 0.45 eV, a value which agrees quite well with the known work functions of these metals. The difference of the work functions decreased with increasing residual gas pressure. The measurements could be reproduced with an accuracy better than two hundreths eV.

Succeeding measurements in metal vapors may give extended information about the behaviour of various adsorption systems in the range of high coverage and minimum work function.

Particular emphasis will be placed on investigating collector materials for thermionic converters employing mixed vapors.

(1) J.B. Taylor and I. Langmuir, Phys. Rev. 44, 423 (1933)

(2) P.M. Marchuk, Trudy Inst. Fiz. Ak. Nauk. Ukraine 7, 17 (1956)

(3) J.M. Houston and K. Dederik, Therm. Spec. Conf. Cleveland (1964)

(4) N.S. Rasor and C. Warner, J. appl Phys. 35, 2589 (1964)

(5) E.P. Gyftopoulos and D. Steiner, Conf. Phys. Electr. MIT (1967)

(6) K.B. Luke and J.R. Smith, NASA-Report TN D-2357 (1964)

(7) V. Bundschuh, Conf. Therm. El. Power Generation, Stresa (1968)

(8) H. Shelton, Phys. Rev. 107, 1553 (1957)

(9) P. Batzies, Conf. Therm. El. Power Generation, London (1965)

(10) P. Kisliuk, Phys. Rev. 122, 405 (1961)

Electron Emission of Molybdenum-Strontium Surfaces

T. Alleau

Centre d'Etudes Nucléaires de Saclay (France) - S.E.P.

Strontium adsorption has already been studied, either alone[1][2] or with caesium[3], but no experimental results were available concerning electron emission, a knowledge of which is necessary for the study of 2-vapour converters. The measurements were made with an electron emission microscope (TEEM) (fig. 1). Strontium is introduced through a pipe drilled in the wehnelt (fig. 2), which can be heated to 1000°C. The temperature is measured by a 5 - 26 % W-Re thermocouple and a micropyrometer. The experimental results are presented (fig. 3) and compared with the Gyftopoulos-Levine-Steiner predictions. The strontium monolayer is found to have a work function of 2.59 eV, which is slightly higher than the values proposed in the literature (2.35 eV). The Gyftopoulos-Levine-Steiner theory enabled these results to be extrapolated to the high current density region (fig. 4), and the strontium pressure needed to obtain 3 eV is found to be of the order of 3 torr.

(1) G.E. Moore and H.W. Allison, J. Chem. Phys. 23, 1609 (1955)

(2) Ya.P. Zingermann, V.A. Ishchuk, and V.A. Morozovskii, Sov. Phys. Sol. St., Vol. 3, Nr. 4 (Oct. 1961)

(3) J. Psarouthakis and R.D. Huntington, Conf. Phys. Elec. M.I.T. (Mass. 1966)

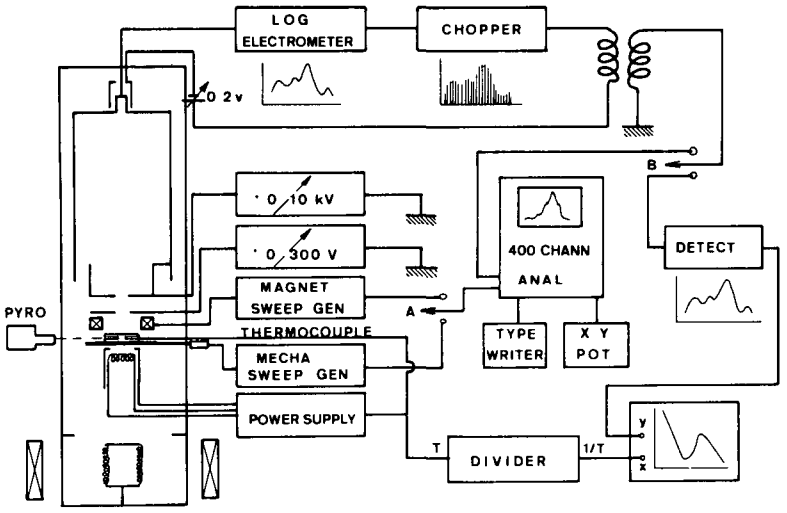

Fig. 1 Schematic of the electron emission microscope (TEEM) and electrical block diagram

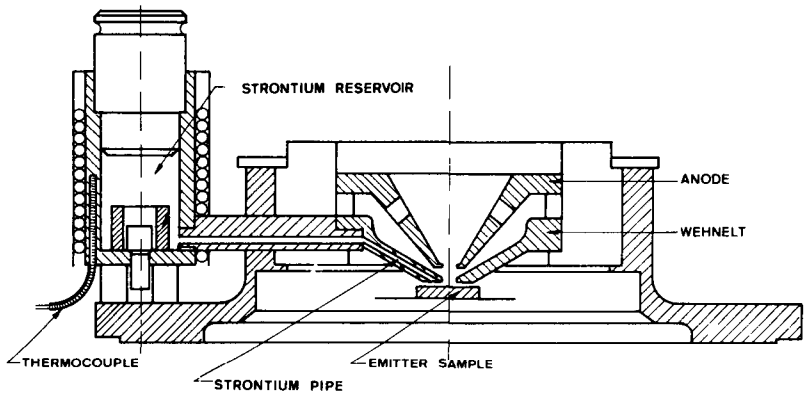

Fig. 2 TEEM and Strontium supply

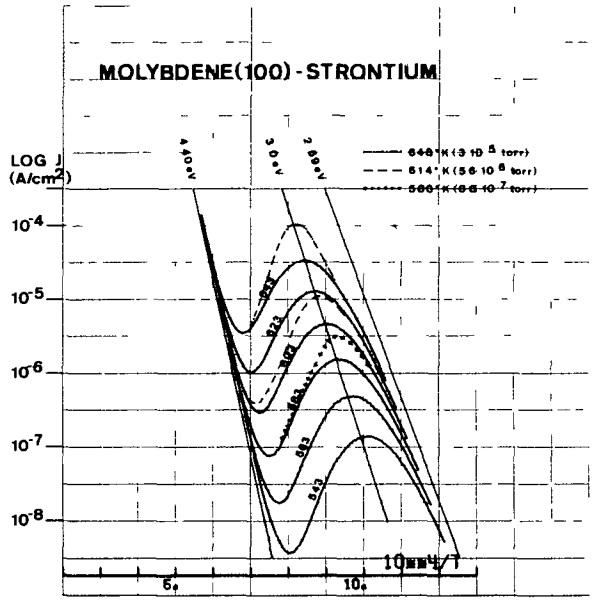

Fig. 3 Comparison between experimental results and the Gyftopoulos-Levine-Steiner theory

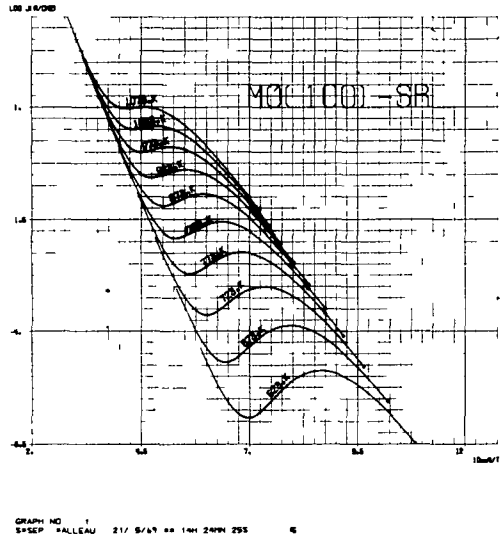

Fig. 4 Extrapolation of the experimental results to higher current densities by the Gyftopoulos-Levine-Steiner theory

W Mo

Stability of Tungsten and Molybdenum Surfaces Heat-Treated in an Atmosphere of Oxygen and Water Vapor

T. Alleau and M. Cornet

Centre d'Etudes Nucléaires de Saclay (France) - S.E.P.

The behaviour of surfaces under electrolytic attack has already been the subject of many publications[1]-[6]. It is now accepted that the electrolytic attack of tungsten in a sodium hydroxide solution reveals etch patterns having (110) oriented faces, of height all the greater as the atomic density of the plane considered is farther from the (110) plane. However heat treatment results, by surface diffusion, in a polishing all the more rapid as the orientation of the basic plane of the substrate is farther from the (001) plane. The aim of the experiments is to preserve the etch aspect longer by changing the surface energy functions through the adsorption of electronegative compounds such as oxygen and water vapour. Thivellier[6] studied this phenomenon from a theoretical viewpoint. The experimental verification began with the heat treatment of polished samples of molybdenum and tungsten, monocrystalline and polycrystalline, under vacuum and temperature conditions ($3 \cdot 10^{-7}$ torr at 2200°K) which prohibit pollution and do not change the surface energies. No modification was observed. A second series of experiments was performed using the same polished polycrystalline surfaces at the same temperature, but with a partial pressure of oxygen (or water vapour) sufficient (10^{-5} torr) to create an atomic layer on the surface. Certain grains then show etch patterns, the orientation planes being found on examination to be close to (112). This confirms the reduction in surface energy and the trend of the total energy function towards that of dense planes (fig. 1+2). A third

series of experiments is in progress and consists in comparing the changes in surfaces attacked electrolytically, during heat treatment, with and without an adsorbed layer.

(1) L. Van Someren, Therm. Conv. Spec. Conf., Cleveland (1964)

(2) D.P. Lieb and G. Miskolczy, Therm. Conv. Spec. Conf., Cleveland (1964)

(3) S.S. Kitrilakis and F. Rufeh, Therm. Conv. Spec. Conf., Houston (1966)

(4) T. Speidel, Therm. Conv. Spec. Conf., Palo Alto (1967)

(5) P. Batzies, J. Demny, and H.E. Schmid (K 5), Therm. Elec. Pow. Gen., Stresa (1968)

(6) D. Thivellier (K 6), Therm. Elec. Pow. Gen., Stresa (1968)

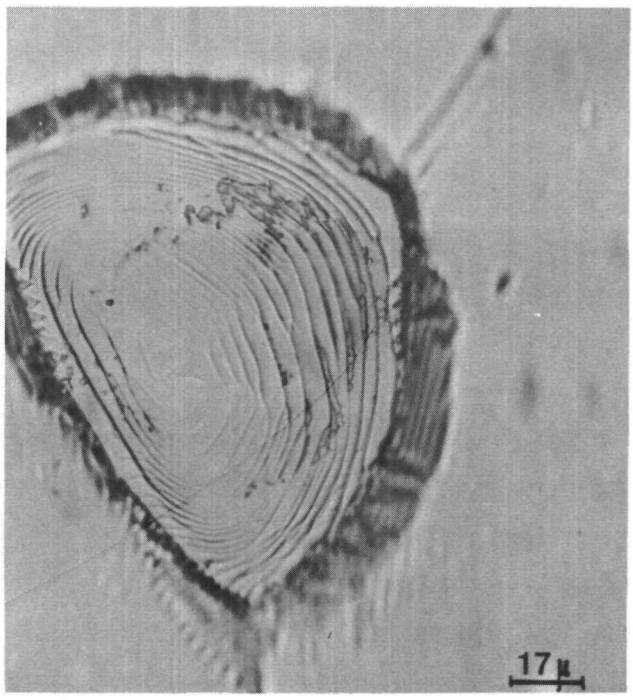

Fig. 1 Tungsten
12^h at 2150^oK, $p(O_2) = 5.10^{-6}$torr

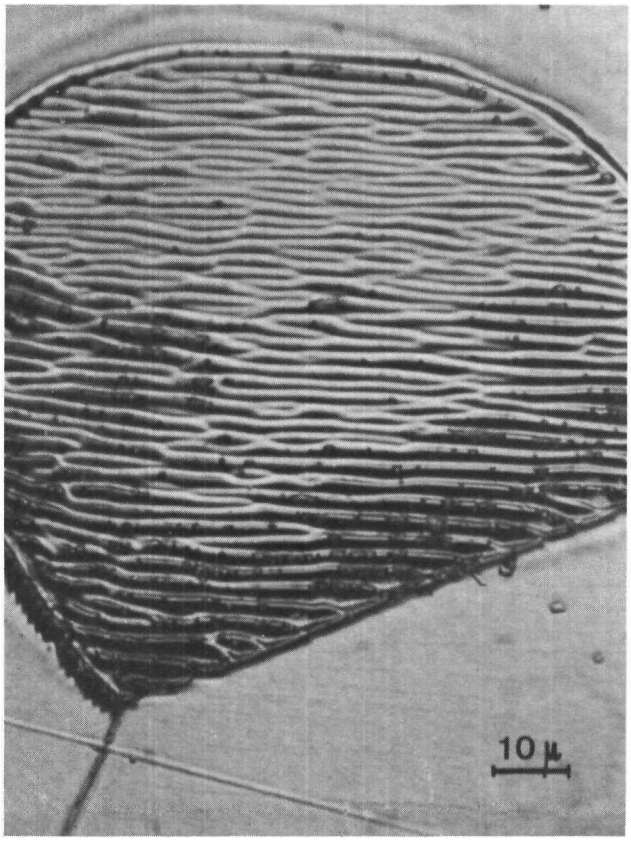

Fig. 2 Tungsten
12^h at 1900^oK, $p(O_2) = 10^{-4}$ torr

Modification of the Work Function by Adsorption of Electronegative Gases

T. Alleau and F. Dumont

Centre d'Etudes Nucléaires de Saclay (France) - S.E.P.

The work function is measured by thermoelectron emission in a TEEM microscope on samples of monocrystalline tungsten, under a known flux of gas molecules[1] (fig. 1).

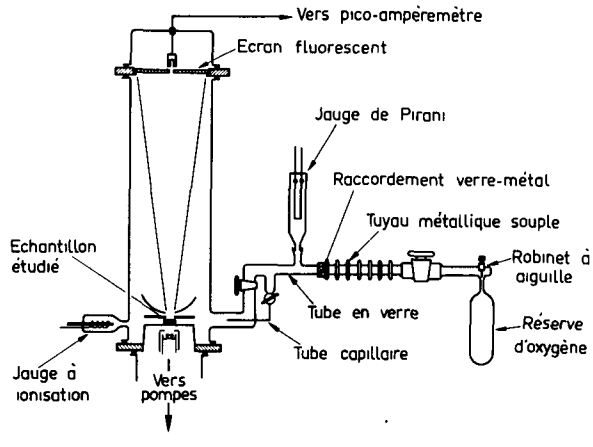

Fig. 1 TEEM and gas supply

1. Oxygen:

Two different processes were observed:
if special care has not been taken in the cleaning and gegassing of the elements of the microscope, adsorption of oxygen leads to the appearance of 3 distinct zones: a clean zone, a high work function zone representing oxygen adsorp-

tion, and an intermediate zone of lower work function than the original surface, this reduction reaching 0.3 eV (fig.2).

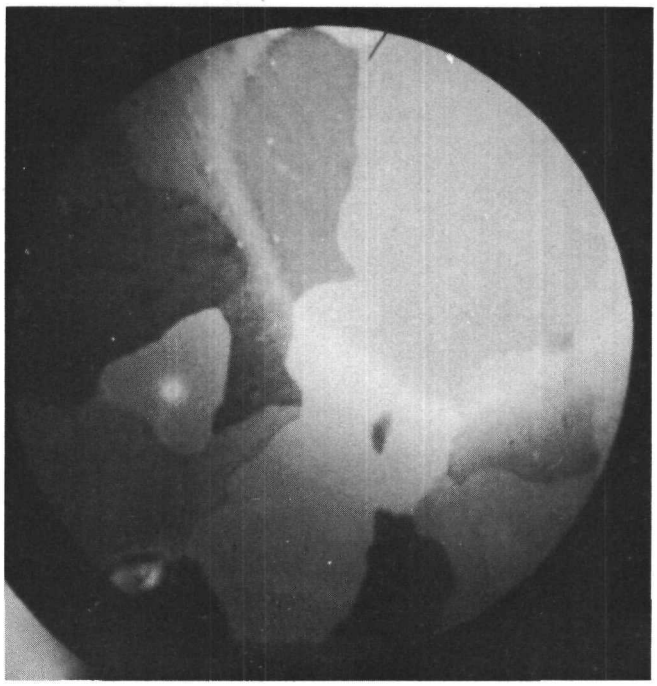

Fig. 2 Oxygen adsorption on tungsten,cloud effects

The explanation of this phenomenon is assumed to lie in the reaction of an impurity, not yet determined with a small concentration of oxygen.

When the gas and the surface are clean, adsorption becomes homogeneous and the results obtained agree with those known in the literature (fig. 3).

2) Nitrogen, Chlorine:

It is shown experimentally that at high temperature these gases have no effect on the work function at pressures up to 10^{-5} torr. This fact can be explained theoretically by comparison of the desorption energies with that of oxygen:

	O_2	N_2	Cl_2
E_d (Kcal/mole)	140	75	81.5

It can be admitted that gas adsorption yields to the Langmuir equation. In the high temperature and low pressure range, the Langmuir equation can be confined to the Henry equation[2].

$$\theta = \alpha . P \exp (E_d/RT)$$

From this expression can be calculated the ratio of the oxygen and nitrogen (or chlorine) coverage under 10^{-5} torr pressure on a tungsten surface at 1850°K for example.

We find:

$$\frac{\theta O_2}{\theta N_2} = 4.7 \cdot 10^7 \qquad \text{i.e.} \quad \Delta\phi = 10^{-7} \text{ eV}$$

$$\frac{\theta O_2}{\theta Cl_2} = 8.1 \cdot 10^6 \qquad \text{i.e.} \quad \Delta\phi = 10^{-7} \text{ eV}$$

To conclude, nitrogen and chlorine have no influence on the working of thermionic converters, on condition that their pressure does not interfere with the path of the electrons.

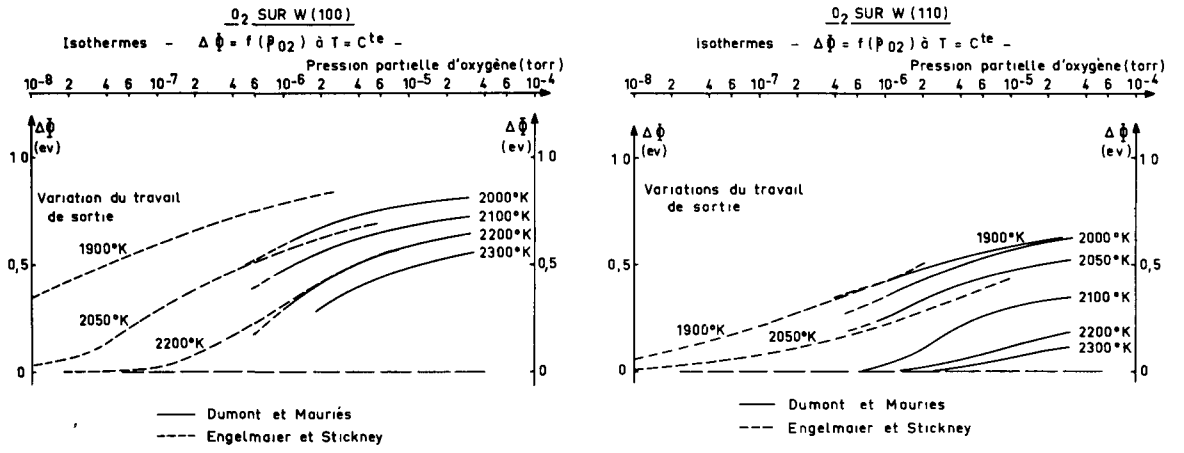

Fig. 3 Work function change for oxygen adsorption on W (100) and W (110)

(1) F. Dumont and J. Mauries (K-10), Therm. Elec. Pow. Gen. (1968) Stresa

(2) S. Brumauer, L.E. Copeland, and D.L. Kantro, "The Langmuir and B.E.T. Theory" - p. 77 in "The Solid Gas Interface", ed. by E.A. Flood